Alma Mater Studiorum – Università di Bologna

DOTTORATO DI RICERCA IN

Biologia Cellulare e Molecolare

Ciclo XXXII

Settore Concorsuale: 05/E2

Settore Scientifico Disciplinare: **BIO/11**

Characterization of the heat-shock circuit in Campylobacter jejuni

Presentata da: Marta Palombo

Coordinatore Dottorato

Prof. Giovanni Capranico

Supervisore

Prof. Vincenzo Scarlato

Co-supervisore

Prof. Stefano L. Ciurli

Esame finale anno 2020

Abstract

This thesis consists of two different works developed on two distinct research themes, both of them included in the broader issue of bacterial virulence.

The first part concerns the molecular characterization of the heat-shock regulatory circuit in the food-borne pathogen *Campylobacter jejuni*. The heat-shock response, being cellular damage protection mechanism, is involved in the establishment of successful infections in different bacteria. Moreover, in *C. jejuni,* this regulatory circuit emerged as a crucial pathway for the shift between commensalism and pathogenicity in different hosts, tanks to the peculiarity to modulate host-pathogen interactions. This evidence makes the heat-shock circuit characterization indispensable to elucidate the molecular basis of *C. jejuni* pathogenicity and virulence.

The second section is inherent to urease activity in the presence of gold-based compounds. The urease enzyme is a virulence factor for different pathogenic bacteria, of which *Helicobacter pylori*, *Mycobacterium tuberculosis*, *Cryptococcus neoformans*, *Yersinia pestis*, and *Proteus mirabilis*. This peculiarity makes the urease an interesting target for potential new specific-drugs against ureolytic pathogens.

Characterization of the heat-shock regulatory circuit in *C. jejuni*

The heat-shock response is a mechanism of cellular protection that triggers a sudden increase in the cellular concentration of different proteins, including molecular chaperones and proteases. This response entails protection against protein folding that is damaged by the stress conditions. In the human pathogen *C. jejuni*, the response to thermic stress is controlled by a regulatory circuit, which acts at the transcriptional level and involves the repressors HspR and HrcA. To characterize the molecular mechanism underpinning HspR and HrcA regulatory function, we investigated in detail the HspR and HrcA interactions with their operator sites by DNase I footprinting assays. These analyses allowed the identification of their binding sites, and highlight a complex architecture resulting from protein-DNA interactions. More in detail, the binding architecture is composed

of multiple HspR-recognition sites located in a singular promoter, added to the HrcA-binding element on co-regulated promoters. Moreover, our results indicate that HspR interacts cooperatively with high and low-affinity DNA binding sites mapping on each promoter. To elucidate the role of this complex DNA-binding, we tested the HspR binding ability to several DNA probes harbouring mutations within the target sequences. We also explored the DNA-binding properties of HspR and HrcA competitively on their common targets and observed for the first time that each regulator has a positive effect on DNA-binding ability of the regulatory partner. This mutual cooperative effect, of HspR and HrcA, on DNA binding could explain the synergic repressive impact of the two repressors observed *in vivo* on co-regulated promoters.

Urease inactivation by gold-based compounds

Urease is an enzyme that plays a crucial role as virulence factor in the pathogenesis of different microorganisms. In this work, we analysed the inhibition ability of different gold-based compounds on urease, investigating the potentiality of these compounds as future antimicrobials in ureolytic bacteria. We implemented different enzymatic assays allowed to kinetically characterize the inhibitory activity of the Au(III)-complexes, and revealing their ability to inactivate the enzyme in the low nanomolar concentration range. Moreover, our results permitted to elucidate the inhibition modality of these compounds, which resulted based on a slow-binding mechanism requiring the two-isomerization steps.

Contents

Characterization of the heat-shock circuit in *C.jejuni*

Introduction

1.1 *Campylobacter jejuni*

Campylobacter jejuni (**Fig.1**) is a Gram-negative, microaerophilic, spiral, and flagellated bacterium belonging to the delta-epsilon group of proteobacteria, in the order *Campylobacteriales*, including also the genera *Helicobacter* and *Wolinella*.

Figure 1: Scanning electron micrograph of *C. jejuni* clinical strain M129 with an INT 407 epithelial cell. Adapted from WSU School of molecular biosciences Konkel & colleagues.

1.1.1 Epidemiology

C. jejuni is the leading cause of bacterial food-borne diarrhoeal disease worldwide (Blaser, 1997), accounting for more infection than *Escherichia coli* O157:H7, *Salmonella* spp. and *Shigella* spp. (Apel, Ellermeier, Pryjma, DiRita, & Gaynor, 2012). While most cases of gastroenteritis associated with *C. jejuni* infection are generally self-limiting, it is also linked to severe post-infection complications, such as Gullian-Barré syndrome, a demyelinating polyneuropathy causing bilateral paralysis (Nyati & Nyati, 2013). Although *C. jejuni* is a human pathogen, it can colonize in an asymptomatic manner the gastrointestinal tract of different animals, including chicken and other avian species. This ability is at the root of its contamination cycle, where contaminated water and unpasteurized milk or meat, especially poultry,

serve as *C. jejuni* reservoirs, and it is a source for human infection (Young, Davis, & DiRita, 2007).

1.1.2 Pathogenicity

Throughout the establishment of an infection, bacteria must overtake the mechanical and immunological barriers of the gastro-intestinal tract. *C. jejuni* succeeds in bypassing the mucus layer of the gastro-intestinal epithelium, the first defence line, because of its motility, corkscrew morphology, and of an unusual lipooligosaccharide. Indeed, *C. jejuni* lipooligosaccharide is made up of relatively short O-sidechain that may reduce nonspecific binding to the mucin glycoproteins (McSweegan & Walker, 1986). After passing the mucus layer, *C. jejuni* interacts with the epithelial host cells and elicits an immune response that differs between human and chicken. In humans, *C. jejuni* can interact with the epithelial cells both through external bond and internalization by the cells. These interactions cause interleukin (IL)-8 production and induce the recruitment of dendritic cells and the subsequent interaction of macrophages and neutrophils with the bacterial cells. The *C. jejuni* interactions with human cells trigger a massive pro-inflammatory response associated with an increase of the cytokines (Young et al., 2007). Dissimilarly, in chicken *C. jejuni* stimulates the production of IL-1β, IL-6, and intracellular nitric oxide synthase by epithelial cells and macrophages, without leading the pathological inflammatory response. This peculiarity allows colonizing chicken in high numbers. Various factors may reduce or redirect the chicken immune response towards tolerance; heterophils and macrophages might also have a role, whereas epithelial cell invasion is not reported (Young et al., 2007).

1.1.2.1 Flagella and chemotaxis in C. jejuni pathogenicity

Among the different *C. jejuni*'s elements that allow it to establish a successful infection, an essential role is exerted by the flagella and flagellar motility, which are involved in host colonization, virulence, host-cell invasion and secretion (Young et al., 2007). The chemotaxis seems to play a crucial role both in commensalism and pathogenicity in *C. jejuni*. Indeed, mutations of the chemotactic genes affect chicken colonization, as well as virulence in pathogenic hosts (Hendrixson & DiRita, 2004)

(Yao, Burr, & Guerry, 1997). Besides, *C. jejuni* displays chemotactic motility towards components of the mucus and amino acid found in the chick gastrointestinal tract (Hugdahl, Beery, & Doyle, 1988).

1.1.2.2 Cytolethal distending toxin

C. jejuni, like other bacterial species, produces cytolethal distending toxin that is linked with the double-strand DNA brakes and the arrest of the cell cycle (Lara-Tejero & Galan, 2000)(Hassane, Lee, & Pickett, 2003). The cytolethal distending toxin is expressed booth in chicken and in human, but in chicken were not found neutralizing antibody agaist the toxin, highlighting a variance in the recognition way by the two hosts (Young et al., 2007).

1.1.2.3 Heat-shock response in *C. jejuni* pathogenicity

An interesting difference between chicken and mammals, including humans, is the body temperature, 42 °C in chicken, and 37 °C in human. This difference could make the temperature a potential signal for host-specific infection, and in turn the heat-shock response a mechanism able to promote the switch between commensalism and pathogenicity (Apel et al., 2012) (Young et al., 2007). Generally, the heat shock response plays a central role in host-pathogen interaction of different bacteria species as a mechanism of cellular protection able to preserve the protein folding, which is damaged by the stress conditions encountered during the establishment of an infection. This makes different heat-shock proteins virulence factors or elements that contribute to pathogenesis in an indirected manner (Roncarati & Scarlato, 2017). In *C. jejuni*, the heat-shock response is mediated by the two transcriptional repressors, HspR and HrcA (Andersen et al., 2005) (Holmes, Penn, & Lund, 2010), which repress transcription of the heat-shock genes at low temperature, 37 °C. Another regulatory system that might be involved in the survival at high temperature is the RacR/RacS two-component system. This system also responds to different environmental conditions encountered during infection, but independent of the temperature switch (Apel et al., 2012). Interestingly, the deregulation of the heat-shock proteins, the transcriptional repressors HspR and HrcA, and the RacRS system is linked to an altered bacterial length causing an elongation of the cell. This

phenotype is also connected to motility defects, and consequently, to a deficiency in epithelial cell invasion. This motility deficiency is caused by filamentation of the cells and does not involve defects in the flagellar apparatus (Andersen et al., 2005) (Apel et al., 2012).

1.1.2.4 Genetic variation and natural transformation

Other *C. jejuni*'s elements relevant to its pathogenicity are the extensive genetic variation and the natural transformation. Intriguingly, the majority of the hypervariable sequences are in regions encoding proteins associated with the production and modification of the surface structure, and involved in immune avoidance, virulence, secretion and invasion of host cells. This class includes capsule, surface polysaccharide, lipooligosaccharide, and flagellar genes (Parkhill et al., 2000)(Linton et al., 2000)(Young et al., 2007). Moreover, *C. jejuni* is naturally competent and can take up DNA from the environment. That leads to recombination between strains, allowing the generation of high genetic diversity. The horizontal transfer of both plasmid and chromosomal DNA occurs both *in vitro* and during chick colonization, indicating that natural transformation could play an important role in genome plasticity and in the spread of new genetic tracts such as antibiotic resistance, even in the absence of selective pressure (De Boer et al., 2002)(Avrain, Vernozy-Rozand, & Kempf, 2004)(Young et al., 2007).

1.1.3 *C. jejuni* genome

C. jejuni has a genome of approximately 1600 kb in size. The genome analysis of *C. jejuni* NCTC11168 strain predicted the existence of 1654 protein-coding genes and 54 stable RNA species (Parkhill et al., 2000). Its genome compared to the genome of the closely phylogenetic related microorganism *H. pylori* shows strong similarity, which, however, is exclusively restricted to housekeeping functions. Indeed, just 55.4% of *C. jejuni* genes show an orthologous in *H. pylori* (Parkhill et al., 2000).

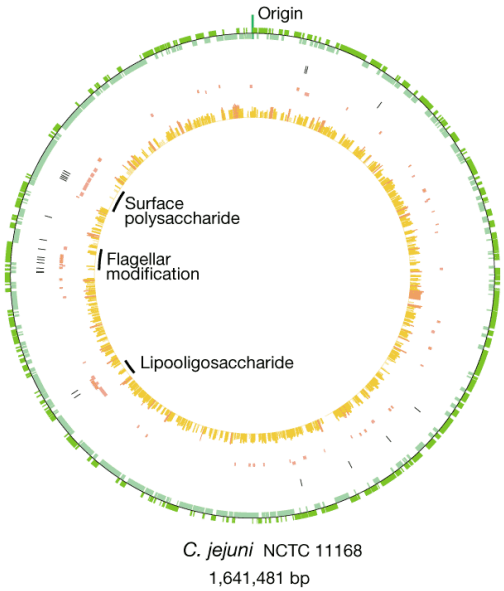

Figure 2: Coding sequences transcribed in the clockwise direction (dark green), and coding sequences in the anticlockwise direction (pale green). It is marked the putative origin of replication. In black the positions of hypervariable sequences are highlight. The genes involved in the production of surface structures are marked (clockwise in dark red and anticlockwise in pale red). The similarity of each gene to its *H. pylori* orthologue is indicated by the height of the bar and the intensity of the colour. Adapted from Springer Nature, License Number: 4698690911335 (Parkhill et al., 2000).

As *H. pylori*, the *C. jejuni* genome sequence shows a low G+C content of 30.6% with two large regions including the portion for the lipooligosaccharide and the extracellular polysaccharide biosynthesis cluster, where the G+C content drops down to 25.4% and 26.5%, respectively (Parkhill et al., 2000). The higher A+T content maps in the proximity of promoter regions. Analysis of these regions carried out in different *C. jejuni* strains showed an extended -10 box with an upstream periodic A/T-rich pattern as a consensus motif in 89% of the promoters. The relationship between this A/T-rich region and their relevance in transcription initiation is also confirmed by the identification of several examples of disruptive single-nucleotide-polymorphisms (SNPs) in the A/T-rich region (Dugar et al., 2013). An A/T-rich sequence followed by the AAGGA-motif is also detected as the consensus sequence for the ribosome binding site. Highlighting the relevance for the A/T-rich pattern even in the mRNA translation (Dugar et al., 2013).

C. jejuni is predicted to code for a higher number of regulatory proteins than *H. pylori,* although a similar genome size. Likely, this may be due to a higher number of

ecological niches colonized by *C. jejuni* (Parkhill et al., 2000). As *H. pylori*, also *C. jejuni* displays only three sigma factors, the housekeeping σ^{70}, and two alternative σ^{54} and σ^{28} sigma factors, which regulate the expression of many flagellar genes (Carrillo et al., 2004) (Dugar et al., 2013). In contrast, the more significant portion of regulatory factors belongs to the two-component regulatory systems (Parkhill et al., 2000). A peculiar feature of *C. jejuni* is represented by a high frequency of genome variation, provided by the high number of hypervariable sequences. Intriguingly, this variability may be linked with slipped-strand mispairing in the proximity of homopolymeric tracts during the replication, and probably linked to the absence of several *E. coli* DNA-repair genes homologues. The high levels of variation observed in the shotgun sequences denote that it is not possible to build a single definitive sequence for the *C. jejuni* genome. As such, it possesses some of the properties of quasi-species; a phenomenon that is well described in RNA viruses (Young et al., 2007) (Parkhill et al., 2000). Another peculiarity of the *C. jejuni* genome is the absence of functional insertion sequence (IS) elements, retrons, transposons, and prophages, except for the Cj0752 insertion sequence that is similar to IS605 *tnpB* from *H. pylori* (Parkhill et al., 2000). The absence of these elements seems to correlate with the presence of a type-II CRISPR/Cas system. Indeed, strains that display degenerated CRISPR loci frequently show plasmids and integrated elements (Dugar et al., 2013).

1.2 Regulatory systems

Generally, bacteria react to changes in environmental conditions or the intercellular state, re-modulating the expression of genes that code for proteins involved in the adaptation to the new state. This response is commonly mediated by transcriptional regulatory circuits, which are switched on by sensors upon detection of the signals. The active sensors are able to transduce the signals to transcriptional factors. This produces a change in the regulators ability to directly interact with DNA sequence on target promoters to activate or repress genes transcription (Perez & Groisman, 2009). These regulatory patterns are bundled in densely connected networks able to modulate the cellular response by interconnecting several stimuli and producing an

accurate output suitable for the specific condition (Seshasayee, Bertone, Fraser, & Luscombe, 2006).

1.2.1 The heat-shock circuit

The heat shock response is a mechanism of cellular protection that implicates the production of different heat-shock proteins, as chaperone and proteases, able to prevent the accumulation and the consequent aggregation of denatured proteins, which occurs during stress conditions, and avoid a toxic effect on the cell (Roncarati & Scarlato, 2017). Although the heat-shock response is a universal phenomenon observed in all studied bacterial species, microorganisms do not use a unique regulatory strategy. Indeed, they have evolved various mechanisms based on both transcriptional and posttranscriptional regulation, and involving both positive and negative mechanisms of regulation (Roncarati & Scarlato, 2017).

A classic example of heat-shock circuit is the *Escherichia coli* positive mechanism that combines a transcriptional and translational regulation. *E. coli* uses two alternative sigma factors, one of them, RpoH, is able to interact with RNA polymerase core enzyme and direct the proteins complex to the promoter region of the heat-shock genes, recognizing specific DNA sequences located in these promoters (Sharp et al., 1999) (Kumar et al., 1995). In this system, the heat-shock response is activated by the increment in the amount of the RpoH alternative sigma factor in response to temperature increase. Indeed, the *rpoH* mRNA region that includes the ribosome-binding site and the AUG start codon acquires a complex secondary structure with high stability at low temperatures. This peculiar mRNA conformation hinders the recruitment of the translation machinery and the consequent translation of the *rpoH* messanger. At 42 °C, a partial misfolding of the *rpoH* mRNA secondary structure occurs and allows the assembling of the ribosome and the consequent efficient translation of the sigma factor (Morita et al., 1999). Moreover, also a post-translational regulatory mechanism monitors the amount of the available RpoH protein to enhance transcription of the heat-shock genes. Indeed, in the absence of denatured protein, different chaperons can interact with the alternative sigma factor and sequester it. Whereas, when the amount of misfolded

proteins increase, the chaperones are recruited by denatured polypeptides, and release the sigma factor (Tomoyasu, Ogura, Tatsuta, & Bukau, 1998). In addition to this chaperon's sponge effect towards the available RpoH, chaperon systems seem to play a crucial role in promoting protease-mediated degradation, fundamental to decrease the alternative sigma factor stability and re-establish the steady-state level (Roncarati & Scarlato, 2017). Although most gram-negative bacteria exploit an alternative sigma factor, other bacteria, among which *C. jejuni* and *H. pylori,* evolved an opposite strategy to control chaperone genes' expression, which is based on a dedicated repressor system. So at 37 °C, the transcription of the heat-shock genes is inhibited by the repressor binding to promoter regions. In contrast, the increase in temperature reduces the repressor affinity for the target DNA and allows the transcription to start (Roncarati & Scarlato, 2017). It is known that the heat-shock circuit in *C. jejuni* is based on two repressors, HrcA and HspR (Andersen et al., 2005)(Holmes et al., 2010). Although a molecular characterization of their DNA-binding activity in *C. jejuni* is not available, there is a variety of information that came from the HrcA and HspR investigation in other bacterial species. In *H. pylori*, the HrcA/HspR circuit was previously characterized, showing a complex regulatory network composed of the master regulator HspR, which directly regulates another regulator (HrcA) and a target gene (*groESL*), which in turn is regulated by both HrcA and the master regulator (HspR). Moreover, considering that all the regulatory interactions are repressive, these circuits seem to represent rare examples of incoherent type-2 feed-forward loops (Danielli, Amore, & Scarlato, 2010)

1.2.1.1 HrcA

The HrcA repressor protein was first identified and characterized in *Bacillus subtilis*, where it was also identified the *cis*-element CIRCE (controlling inverted repeat of chaperons expression), an inverted repeat (IR) necessary for the binding of HrcA to the target genes promoters (A. Schmidt, Schiesswohl, Volker, Hecker, & Schumann, 1992) (Schumann, Homuth, & Mogk, 1998). Afterward, different studies tried to obtain the biochemical identification of HrcA-CIRCE interaction at a molecular level. Unfortunately, this characterization has been possible only in *H. pylori* and *Chlamydia trachomatis*, because of the high HrcA instability and its propensity to

aggregate in insoluble bodies (Roncarati, Danielli, Spohn, Delany, & Scarlato, 2007) (Roncarati, Spohn, et al., 2007) (Wilson & Tan, 2004). The available information about the HrcA interaction with promoters shows the repressor-binding region mapping close the transcription start sites. This evidence indicates that HrcA exerts its repressive function by interfering with the transcriptional machinery, occluding the RNA polymerase binding site on the heat-shock promoters at 37 °C (Roncarati & Scarlato, 2017). HrcA loses DNA-binding affinity upon a temperature increase, and releases the operator allowing the binding of the RNA polymerase and transcription. The mechanism by which HrcA can sense heat-shock conditions is based on the ability of the chaperon GroE to enhance the repressor binding ability (Schumann et al., 1998). Indeed, this GroE positive effect can take place only at normal grow temperature, when the amount of denatured proteins is relatively low. By contrast, the increment of damaged proteins, as a consequence of the stress condition, produces chaperon recruitment, including GroE, with the consequent stop of its HrcA stimulating activity (Roncarati & Scarlato, 2017). Besides, in *H. pylori*, it was demonstrated that HrcA is also an intrinsic heat-sensing protein. Indeed, this protein showed thermal stress high sensitive structure, which allows the activity of the folded repressor only under heat-shock temperature (Roncarati, Danielli, & Scarlato, 2014). Interestingly, in *Rhodobacter capsulatus*, it was observed that the CIRCE element could also exert an extra function, affecting transcript stability at low temperature, through the formation of a secondary structure promoted by the inverted repeat (Jäger, Jäger, & Klug, 2004). Although HrcA is found in various bacteria, the sequence similarity among proteins from different species is low, generally less than 30%. However, the degree of similarity increases in highly related microorganisms. Interestingly, the similarity is restricted to three short amino acid regions, likely suggesting their essential role to the repressor activity (Morimoto, 1998). The high HrcA instability compromised its structural determination; therefore, limited information is available nowadays. The only protein architecture characterized comes from the *Thermatoga maritima* HrcA crystal structure. Unfortunately, *T. maritima* expresses an inactive form of this protein, unable to bind to the DNA. However, this structure reveals a dimeric form, where each monomer is composed of a helix-turn-helix (HTH) N-terminal DNA-binding domains (DBD), a central domain probably involved in dimerization, and a

C-terminal inserted dimerizing domain (Liu et al., 2005).

1.2.1.2 HspR

HspR is a transcriptional repressor showing amino acid similarities to members of the MerR family of protein regulators. HspR was first identified in *Streptomyces coelicolor*, where it was demonstrated its ability to bind three inverted repeats, named HAIR from HspR associated inverted repeats (Bucca, Hindle, & Smith, 1997) (Bucca et al., 1997). Then, the HspR-HAIR system was found and characterized in diverse bacterial species. In several cases, the HAIR sequences were identified in proximity to the core promoter region (Grandvalet, De Crécy-Lagard, & Mazodier, 1999) (Stewart et al., 2002), a position compatible with a mechanism of repression exerted by a steric hindrance of the RNA polymerase to the promoter region (Spohn et al., 2004) (A. Schmidt et al., 1992). In *H. pylori,* HspR represses transcription of some promoters in conjunction with the HrcA repressor (Roncarati & Scarlato, 2017). Surprisingly, on these promoters the HAIR sequences are located upstream of the transcriptional machinery binding site. This peculiarity suggests a different repressing strategy in the HspR/HrcA co-regulated promoters, if compared with the HspR only regulated ones (Roncarati & Scarlato, 2017). Specifically, HspR interactions occur far upstream of the core promoter elements on HspR/HrcA co-regulated promoters, while -35/-10 boxes are obstructed by HrcA binding (Roncarati, Danielli, et al., 2007). Another HspR feature is its high propensity to oligomerize, which results in extended DNA-binding regions (Spohn et al., 2004). The elaborate arrangement of the binding sites identified on the co-regulated promoters, in addition to the HspR high oligomerization tendency, suggests a complex DNA binding architecture able to finely regulate heat shock gene expression (Spohn et al., 2004). The mechanism by which HspR can respond to heat-shock, and decrease its DNA binding activity is not completely explained. Also, for this heat-shock repressor it is postulated a homeostatic control by chaperones (Roncarati & Scarlato, 2017), as confirmed by the DnaK ability to stimulate HspR DNA binding in *S. coelicolor* and in *M. tuberculosis* (Bucca, Brassington, Schönfeld, & Smith, 2000) (Parijat & Batra, 2015), and by the GroE involvement in the HspR activation in *M. tuberculosis* (Das Gupta, Bandyopadhyay, & Das Gupta, 2008).

Oppositely, in *H. pylori* the heat shock protein CbpA shows a negative effect on the HspR repressor activity. Intriguingly, this function occurs only when the repressor is not bound to the DNA target, revealing a fine regulatory mechanism to limit the heat-shock response (Roncarati, Danielli, & Scarlato, 2011).

Aim of the project

The heat-shock response is a mechanism of cellular protection, which bacteria adopt to face the stress conditions able to compromise the protein folding. This response results in a fast expression of heat-shock genes with the consequent increase in chaperones and proteases amount. The characteristic of being involved in the preservation of the intracellular environment makes the heat-shock regulatory circuit a crucial pathway during the establishment of host-pathogen interactions when the microorganism is subject to different stress damages. Moreover, there are indications that heat-shock proteins may play a role in host-specific infection in the food-borne pathogen *C. jejuni*. Besides, the heat-shock circuit ability to sense temperature changes makes this response a potential mechanism by which *C. jejuni* can switch between commensalism in the chicken reservoir and pathogenicity in humans. Although the heat-shock circuit is investigated in different bacteria species, the molecular characterization of this response is not available for *C. jejuni*. The purpose of this work is to elucidate the transcriptional regulatory modality by which the pathogen can fine regulate chaperons and proteases expression, clarifying the molecular mechanisms on the roots of this central response. With this purpose and starting to the involvement of the heat-shock two transcriptional repressors, HspR and HrcA, in the regulatory circuit of *C. jejuni*, their interactions with potential operators are investigated in detail by DNase I footprinting assays. Moreover, the HspR complex DNA-binding architecture is elucidated, analyzing the regulator interacting ability with several mutants of the promoter sequences. Furthermore, the HspR/HrcA co-regulation is explored on the common target by DNA *in vitro* binding assays under competitive conditions. Different protein-protein interaction assays are also performed to clarify the homo- and hetero-oligomerization ability of the two repressors involved in the regulatory circuit.

Results

3.1 Investigation of the *Cj*HspR heat-shock promoters target interaction

Previous studies identified the *C. jejuni* HspR regulon with a microarray approach, comparing transcript levels of wild type and a Δ*hspR* mutant strain (Andersen et al., 2005) (Holmes et al., 2010). The analysis highlighted thirty deregulated transcripts, seventeen of which appeared downregulated, and thirteen were upregulated. A further bioinformatics analysis was applied to identify putative HspR binding sites in proximity of deregulated promoters. Sequences with similarities to the HAIR-sequence motif from *Streptomyces ssp* were identified in four promoter regions, inferring the operons carrying these motifs as putative direct targets of HspR in *C. jejuni*. **Figure 3** shows a schematic representation of these operons, consisting of the *Pcbp*, *Pclp, Pgro*, and *Phrc* promoters, which control transcription of the major chaperone and *hrcA* and *hspR* regulatory genes. The scheme also displays the positions of the HAIR-like motif in the promoter regions. However, the functionality of HAIR-like sequences is not supported by experimental evidence, and a mechanism able to explain the HspR transcriptional repression effect is not identified (Andersen et al., 2005) (Holmes et al., 2010).

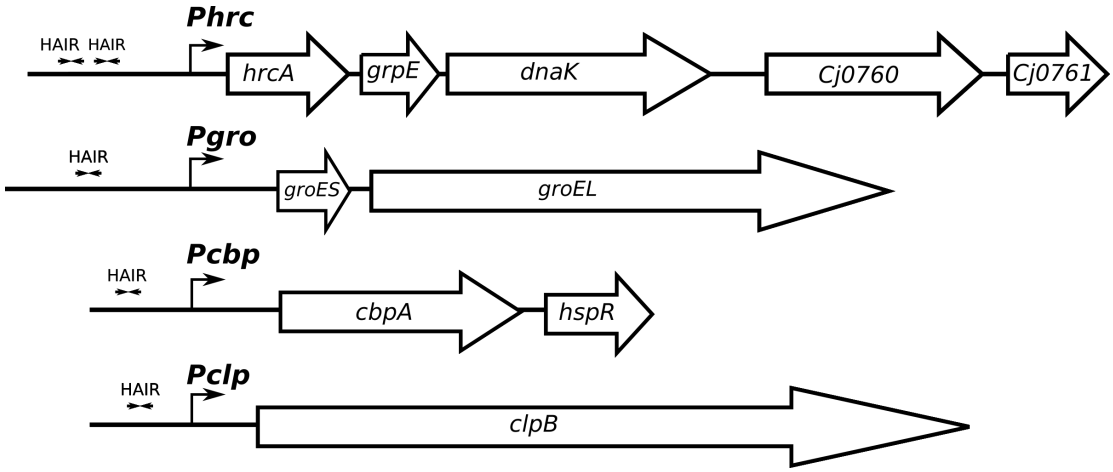

Figure 3: Schematic representation of the chaperone genes in *C. jejuni*. Open arrows indicate coding genes. HAIR-like motifs are represented by convergent arrows. Bent arrowed indicate the start sites of transcription at the indicated promoters.

To start the characterization of *Cj*HspR binding on these regions, and explore the role of the identified HAIR-like sequences in repressor binding, we set up DNase I footprinting assays with purified recombinant *Cj*HspR on the *Pcbp*, *Pclp, Pgro*, and *Phrc* promoter probes. Initiation of RNA transcription on these promoters was identified by RNA-sequencing with a SuperGenome approach (Dugar et al., 2013) and verified in this study by primer extension analyses (data not shown).

3.1.1 *Cj*HspR interacts with multiple sites of the heat-shock promoters

To demonstrate the direct interaction of *Cj*HspR to the potential target promoters, increasing concentrations of purified recombinant *Cj*HspR were incubated with radiolabeled DNA probes spanning the *Pcbp*, *Pclp, Pgro*, and *Phrc* promoter regions and then digested with DNase I and fractionated on polyacrylamide denaturing gel. The result (**fig. 4**) is consistent with a DNase I footprinting assays obtained when the binding of a protein on the DNA probe occurs. Data reported in the figure clearly shows that upon increase of the amount of CjHspR in the reaction, area of DNase I protection are detected, due to the binding of the protein that precludes DNase I cut. In addition, binding of the protein give rise to the appearence of bands of

hypersensitivity to DNase I, likely an effect of structural DNA changes determined by the binding of the protein.

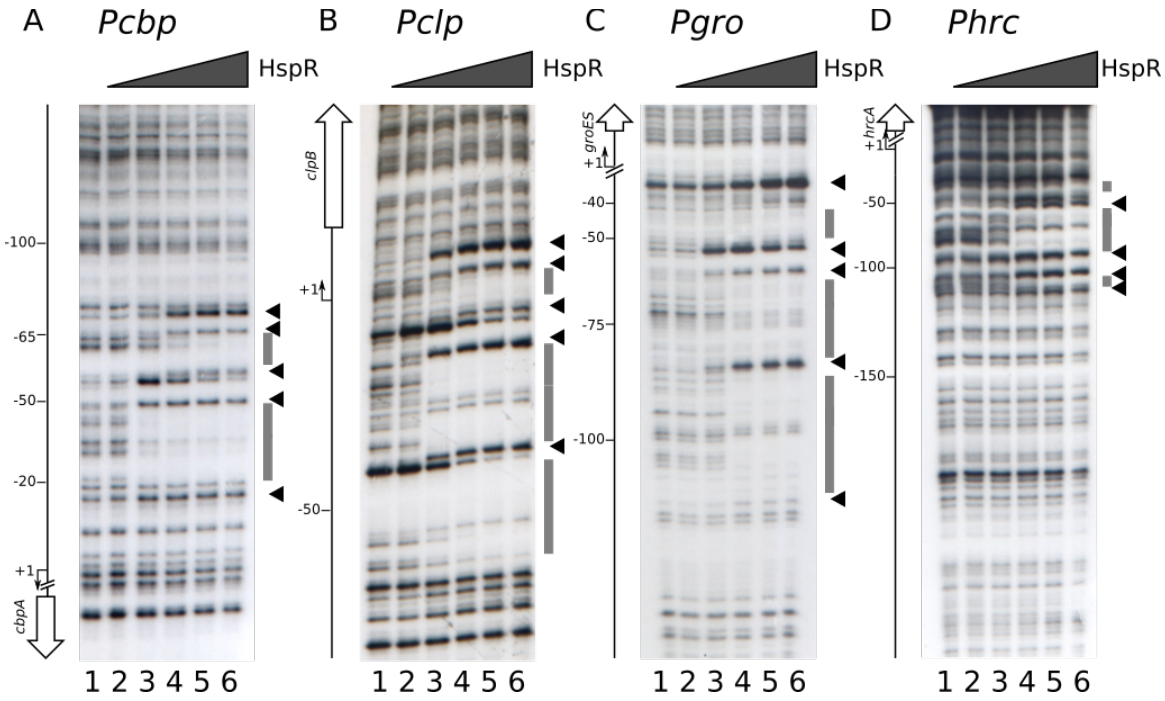

Figure 4: High resolution mapping of *Cj*HspR binding sites on heat-shock promoters. DNase I footprinting assays of *Cj*HspR on P*cbp*, P*clp*, P*gro* and P*hrc* promoter probes (panels A, B, C and D, respectively). Radiolabelled DNA probes were incubated with increasing concentrations of the HspR recombinant protein (0, 11, 22, 45, 90 and 180 nM *Cj*HspR; lanes 1 to 6, respectively) at room temperature and subjected to limited DNase I digestion. In each panel, on the right the grey boxes highlight regions of DNase I protection and the black arrowheads indicate bands of hypersensitivity to DNase I digestion; while on the left, bent arrows indicate the transcriptional start site and vertical open arrows depict the open reading frames; numbers refer to the positions with respect to the transcriptional start sites.

The experiment carried out on the *Pcbp* promoter probe shows protection from DNase I digestion between the position -50 and the -20 above the transcriptional start site (Panel A, lanes 3-6). Also, two bands of hypersensitive DNase I sites appear in proximity of position -50 (lane 3). Upon addition of increasing concentration of *Cj*HspR in the reaction, a second area of protection and two additional hypersensitive bands close to position -65 (lanes 4-6) were detected. A similar result was obtained on the *Pclp* promoter probe (panel B), where the experiment

displayed a protected region with flanking hypersensitive bands (lanes 3). Moreover, an area of protection emerges at high *Cj*HspR concentration (lanes 4-6), and three hypersensitive bands is detected, two of which in the proximity of position +1. Besides, a protection region and hypersensitive bands are visible upstream to the -50 position. The DNase I footprinting assay on the *Pgro* (panel C), instead, shows two bands of DNase I hypersensitivity mapping to the position -50 and the -80 at lower repressor concentration (lane 3-6), and two protected regions between the -50 and -110 at higher *Cj*HspR concentration (lanes 4-6). Finally, additional hypersensitive bands close to the position -40 (lanes 4-6) with an adjacent protection region (lanes 5-6) appear. On the *Phrc* promoter probe (panel D), hypersensitivity bands are identified close to the position -90 at low repressor concentration (lanes 3-6) with a protection region between the position -90 and the -55 (lanes 4-6). Increasing *Cj*HspR concentration, two hypersensitivity bands appear between the position -100 and the -110 (lanes 4-6) with a protection region in proximity to the position -110. Moreover, an additional band tightly the -50 (lanes 3-6) and a protection region near the -30 is exhibited at higher protein concentration (lane 6). Of note, the protection pattern of *Cj*HspR on the DNA probes show an interacting region already at lower protein concentration with additional binding areas detectable at higher protein concentration, suggesting the presence of high and low-affinity binding sites. In summary, low- and high-affinity binding sites are identified on the *Pcbp* and *Pclp.* Differently, a central high-affinity binding site with two flanking low-affinity sites are detected on the *Pgro* promoter. In contrast, the *Phrc* reveal a central high-affinity site with a closely low-affinity binding-site and a potential very low-affinity site.

3.1.2 Analysis of the HAIR-like motif sequence in *C. jejuni*

The HAIR motif proposed as a consensus sequence for the HspR protein of *S. coelicolor* is constituted by IR spanning 21 bp (CTTGAGT-N7-ACTCAAG) (Grandvalet et al., 1999). Inspection of the DNA regions interacting with *Cj*HspR revealed the presence of five HAIR-like sequences in addition to the previously reported HAIR-like sequences (Andersen et al., 2005) (Holmes et al., 2010) (**fig. 3**). Of these, two HAIRs map in the *Pcbp* and *Pclp* promoter regions and three HAIRs are located on

Pgro and *Phrc* promoters. The nucleotide sequences of the four promoters (*Pcbp*, *Pclp*, *Pgro*, and *Phrc*) and their key regulatory elements are summarized in **figure 5**. Strikingly, while the HAIR-like sequences span over the *Pcbp*, *Pclp*, and *Phrc* core promoter elements (-10 and -35 boxes), no HAIR-like sequences overlap the *Pgro* promoter region, mapping upstream of the -35 region. This distinct binding architecture on the promoter regions suggests diversified mechanisms of repression exerted by *Cj*HspR.

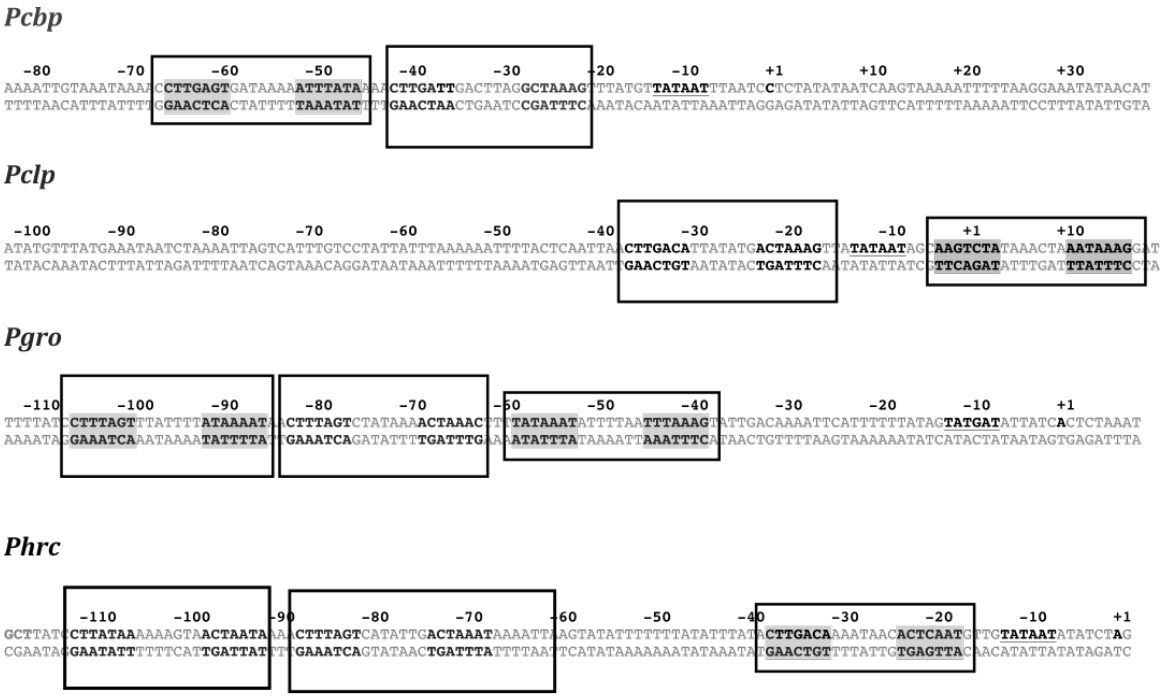

Figure 5: Features of the *Pcbp*, *Pclp*, *Pgro* and *Phrc* promoter sequences. For each is indicated the promoter sequence, and numbers are referred to the transcriptional start site (+1). The -10 and 35 boxes are underlined bold on the coding DNA strand. The HAIR-like sequences are represented in boldface. The HAIR-like sequences identified in this study are grey highlight. The DNase I protection regions are highlight with boxes with different size, where the height is indication of HspR binding affinity for the specific region.

To gain insight on the role of the HAIR-like motif and identify key conserved nucleotides for *Cj*HspR binding, HAIR sequences were aligned and submitted to WebLogo computer program with results shown in **fig. 6**. Alignment of all HAIR sequences highlighted nucleotides conservation within an imperfect IR of 21 bp. The most conserved nucleotides are the first three of the left emisite, CTT. Instead, the right emisite appears less conserved, and the higher conserved nucleotides are one

T and one A, which are, however, rather widespread as compared o the three nucleotides conserved in the left emisite (panel A). Restricting the analysis to the HAIR sequences found in high-affinity *Cj*HspR binding sites, the dissimilarity of the two portions of the inverted repeat decreases (panel B), suggesting that the differences between the high- and low-affinity HAIR may reside in the right IR emisite conservation.

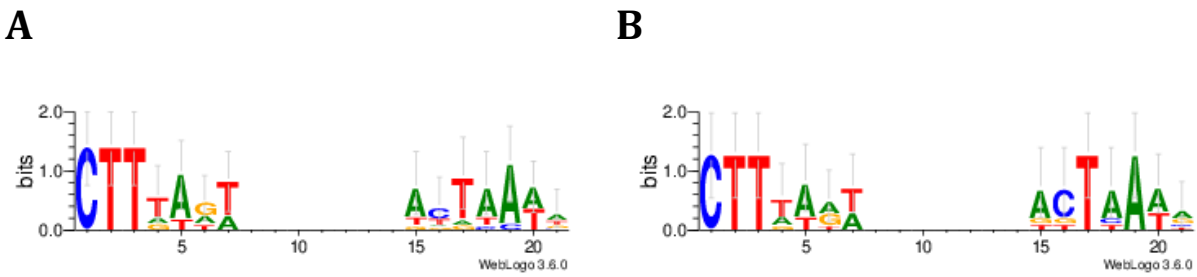

Figure 6: : WebLogo representations of the HAIR sequences characterized through DNase I footprinting assays, **A:** all identified HAIR sequences, **B:** HAIR sequences of high affinity binding sites.

3.1.3 Elucidation of the repressor binding architecture and the binding-site hierarchy

The above study on *Cj*HspR-DNA interaction revealed an intriguing scenario based on multiple binding elements associated with each promoter and showing a variable propensity to interact with the repressor. The HAIR sequence analysis suggests that the diversity in protein interaction ability might reside in the different conservation of the two emisites. To investigate the relevance of the two portions of the HAIR motif, we generated mutants of one or both emisites, and assayed their interacting ability to *Cj*HspR by DNase I footprinting experiments (**fig. 7**). Specifically, we selected the *Pcbp* and *Pgro* promoters for the analysis, as representatives of two different binding architectures for *Cj*HspR. *Pcbp* shows a promoter-proximal high-affinity binding site and an upstream low-affinity site. At the same time, *Pgro* carries a central high-affinity binding site flanked by two low-affinity sites, all upstream of the core promoter region. Base substitutions were applied to the high-affinity binding sites by changing each

base/position and maintaining the same base composition. A representation of the constructed mutants is depicted in **figure 7** (**1**).

1

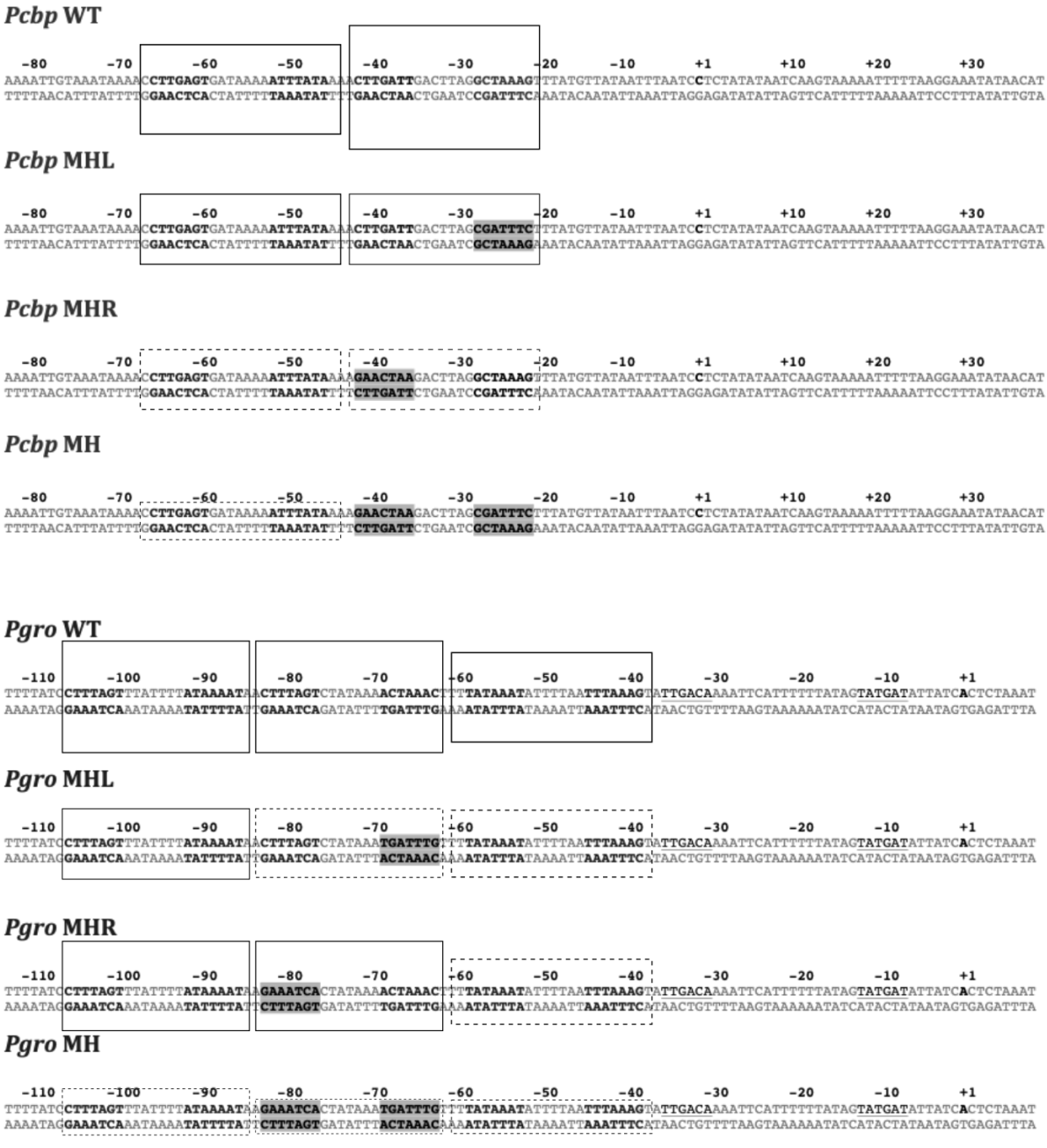

2

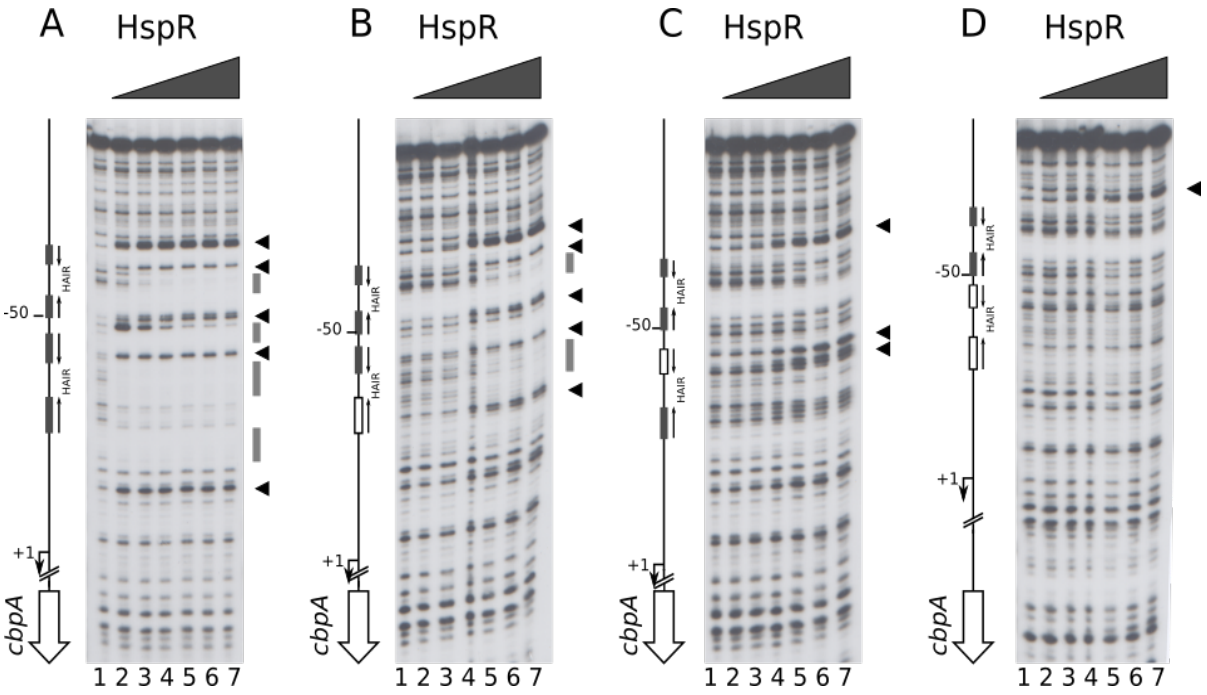
A
HspR
B
HspR
C
HspR
D
HspR
-50
+1
HAIR
cbpA
1 2 3 4 5 6 7

3

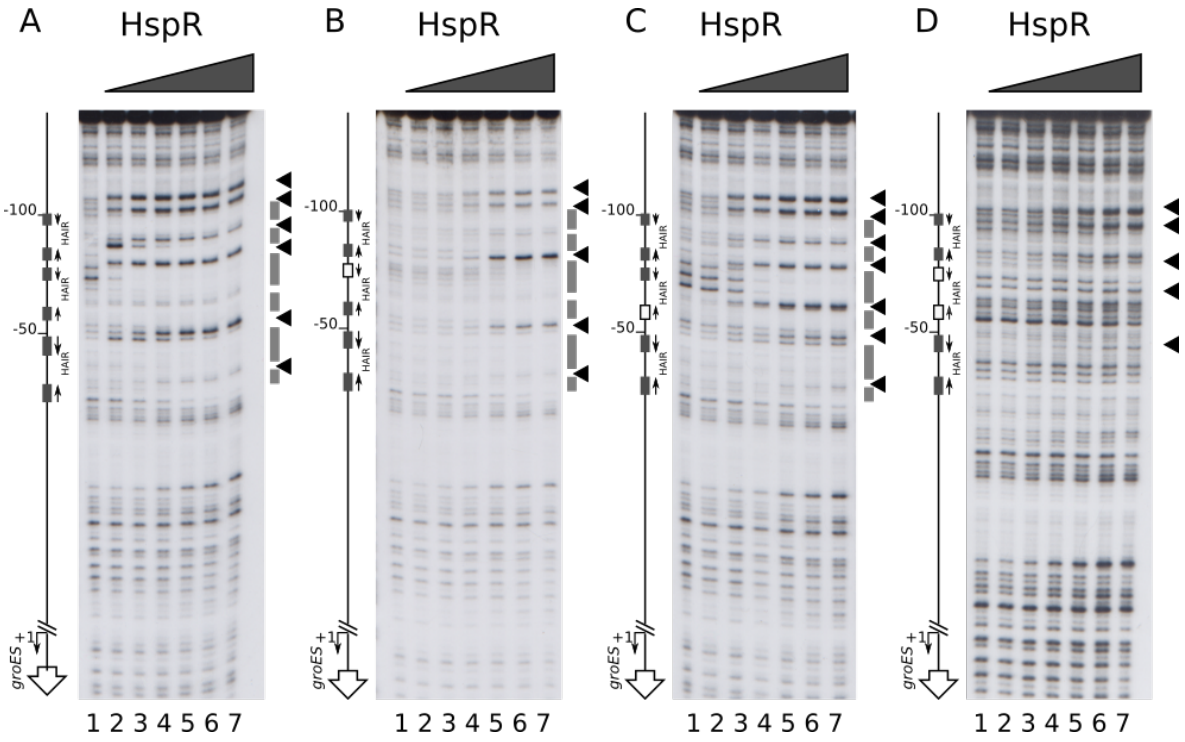
A
HspR
B
HspR
C
HspR
D
HspR
-100
-50
+1
HAIR
groES
1 2 3 4 5 6 7

Figure 7: Features of the *Pclp* and *Pgro* wild type or mutants promoter sequences (panel 1). For each are indicated promoter sequence, and numbers are referred to the transcriptional start site (+1). The HAIR-like sequences are represented in boldface, and the mutated sequences are grey highlight. DNase I footprinting assays of *Cj*HspR on wild type P*cbp* (panel A) or on mutants MHL (panel B), MHR (panel C) and MH (panel D) probes (pannel2), and on wild type P*gro* (panel A) or on mutants MHL (panel B), MHR (panel C) and MH (panel D) probes (panel 3). Radiolabelled DNA probes were incubated with increasing concentrations of recombinant *Cj*HspR protein (0, 22, 45, 90, 180, 360 and 720 nM *Cj*HspR; lanes 1 to 7) at room temperature and subjected to partial DNase I digestion. On the right of each panel, grey boxes depict the regions of DNase I protection and black arrowheads indicate bands of hypersensitivity to DNase I digestion. On the left, schematic representation of the promoter region, where the bent arrows indicate the transcriptional start site, vertical open arrows depict the open reading frame; numbers refer to the positions with respect to the transcriptional start sites. Grey boxes represent the wild type HAIR sequences, while empty boxes represent the mutated sequences.

Comparing the DNase I footprinting assays results of *Cj*HspR on *Pcbp* (**2**) wild type (panel A) to mutant probes (panels B, C, D), it emerged that mutation on one or both portions of the HAIR elicits loss of *Cj*HspR protection. A partial loss of HspR affinity is visible in the mutant of the less conserved "right" emisite of the HAIR (probe MHR, panel B). Differently, the mutation of the more conserved "left" emisite (probe MHL, panel C) produces a more severe loss in protein affinity, which is reflected in a light protection region with three hypersensitive bands, and detectable only with higher HspR concentration. This result highlights a possible key role of the more conserved left emisite in the recruitment of the repressor on the *Pcbp*. Finally, mutations of both HAIRs emisites (probe MH, panel D) abolish almost totally the *Cj*HspR binding to the site and allow the appearance of one residual hypersensitive band at extremely high HspR concentration. An analogous result was obtained on the *Pgro* promoter probe (**3**), where, however, the mutation on one of the two HAIR portions elicits a more gradual loss of *Cj*HspR protection, if compared with the same mutation in *Pcbp* promoter. This allows appreciating the distinct effect generated by the specific mutations, harsher in the case of mutation on the more conserved "right" emisite (MHR, panel B) than in the "left" emisite (MHL). The consequences of mutations on one of the two emisites appear to be less strict on *Pgro* promoters then on *Pcbp*, presumably because of the presence of two low-affinity HAIR sites flanking the one mutated in the *Pgro*. Complete disruption of the high-affinity HAIR (MH, panel D) determined total loss of *Cj*HspR protection pattern.

These results demonstrate that *Cj*HspR binging to DNA requires a full HAIR motif and that mutations on the high-affinity HAIR also determine a severe reduction of *Cj*HspR interaction with the low-affinity binding site. Nevertheless, these results are not sufficient to explain the role exerted by the additional HAIRs on the promoters. To grasp information on the function of multiple *Cj*HspR binding sites on regulated promoters, we performed DNase I footprinting experiments on the *Pgro* promoter mutated in each HAIR motif (**fig. 8**).

1

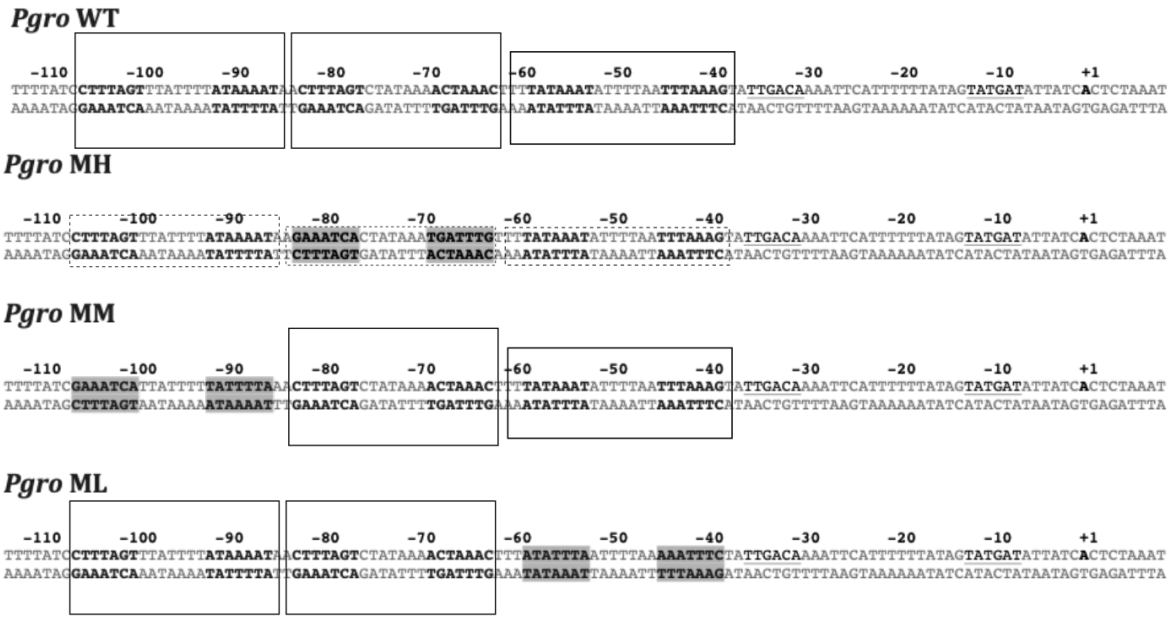

2

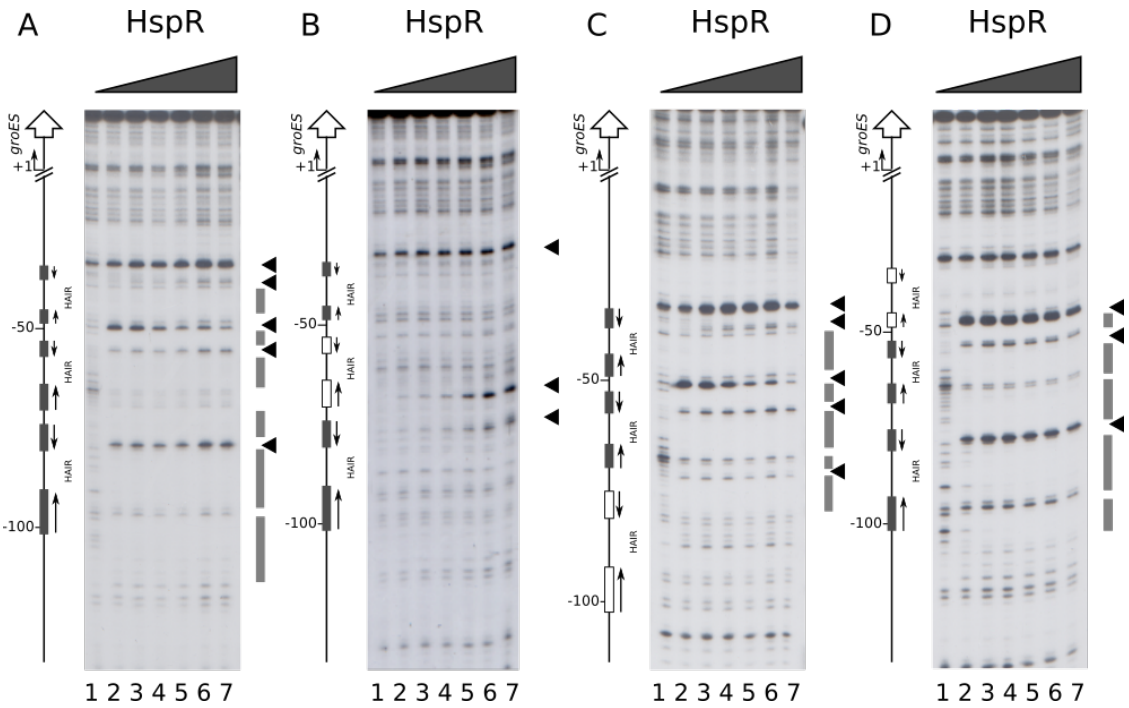

Figure 8: Features of *Pgro* wild type or mutants promoter sequences (panel 1). For each is indicated promoter sequence, numbers are referred to the transcriptional start site (+1). The HAIR-like sequences are represented in boldface, and the mutated sequences are grey highlight (1). And DNase I footprinting assays of *Cj*HspR on wild type P*gro* or mutants MH (panel B), MM (panel C) and ML (panel D) probes (panel 2). Radiolabelled DNA probes were incubated with different concentrations of recombinant *Cj*HspR protein (0, 22, 45, 90, 180, 360 and 720 nM HspR; lanes 1 to 7) at room temperature and subjected to partial DNase I digestion. On the right of each panel, grey boxes depict the regions of DNase I protection and black arrowheads indicate bands of hypersensitivity to DNase I digestion. On the left, schematic representation of the promoter region, where the bent arrows indicate the transcriptional start site, vertical open arrows depict the open reading frame; numbers refer to the positions with respect to the transcriptional start sites. Grey boxes represent the wild type HAIR sequences, while white boxes represent the mutated sequences.

The DNase I footprinting experiment results displays how disruption of the central high-affinity HAIR (MH, panel B) determined a drastic loss of the DNase I protection pattern by *Cj*HspR. This evidence highlighted the essential role of the central high-affinity HAIR for the recruitment of the transcriptional repressor on the promoter. In contrast, DNase I footprinting assays on promoter probes carrying mutations in the two low-affinity HAIR motifs (MM, panel C and ML, panel D) exhibited a drastic loss of *Cj*HspR binding

affinity exclusively for the mutated sequences, without altering the protection pattern on the remaining unaltered binding sites (C and D). This finding reveals that the flanking low-affinity HAIR motifs are not necessary for *Cj*HspR interaction with high-affinity HAIR sequences. Moreover, the observation that a high-affinity HAIR site is required for the repressor recruitment on the promoter highlights the fundamental role that the high-affinity HAIR-*Cj*HspR interaction has to enhance the repressor binding with close low-affinity site. Moreover, these results underline a binding hierarchy among the HAIRs located in a single promoter and depending not only on IR sequence conservation but also on the binding sites reciprocal position. This evidence suggests a potential role for the *Cj*HspR-*Cj*HspR intermolecular connections that might occur between repressors closely bound on the same promoter, and aimed to stabilize the repressor-promoter interaction.

3.2 Characterization of the *Cj*HrcA binding on heat-shock promoters

In the same studies mentioned above, a microarray approach, was carried out to define the *C. jejuni* HrcA regulon. This whole transcriptomic approach was combined with an *in silico* search of putative *Cj*HrcA binding sites looking for sequences with similarities to the CIRCE-sequence motif from *B. subtilis* in the proximity of deregulated promoters. Specifically, the *C. jejuni* NCTC 11168 genome was analysed for the presence of CIRCE-like elements using fuzznuc program from EMBOSS ("the European Molecular Biology Open Software Suite"), leading to the identification of only one putative *Cj*HrcA operator located in the *Pgro* promoter region (Holmes et al., 2010). It is worth mentioning that an additional CIRCE element situated in the *Phrc* promoter has been previously proposed (Thies, Karch, Hartung, & Giegerich, 1999). **Figure 9** reports a schematic representation of the two potential target operons mentioned above. Starting from this information, we focussed our efforts on the study of *Cj*HrcA-DNA binding ability on both the promoters, through *in vitro* DNA-binding assays.

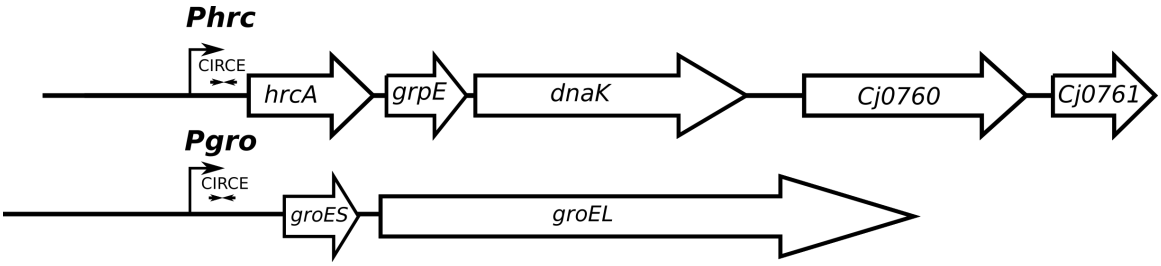

Figure 9: *hrc* and *gro* operons' schematic representation, the two potential CIRCE sequences are indicated on the promoters regions. Symbols are as in the legend to fig. 3.

3.2.1 *Cj*HrcA specifically binds to *Pgro* and *Phrc* promoters

To investigate *Cj*HrcA direct interaction with previously proposed CIRCE elements, we used the *Pgro* and the *Phrc* promoter regions as a probe for *in vitro* binding to a purified *Cj*HrcA protein in DNase I footprinting assays. **Figure 10** shows the *Cj*HrcA ability to bind and protect defined portions of the two probes. The protected regions overlap with the potential CIRCE elements on both promoters. More in detail, the DNase I footprinting experiment on *Pgro* (**Figure 10**; **panel 1**, **A**) shows three bands of hypersensitivity to DNase I digestion, which appear starting from lanes 2 and 3, and two DNase I protection regions noticeable from lane 4 and overlapping the transcriptional start site (+1 position). **Figure 10**; panel **1**, **B** shows that upon the addition of *Cj*HrcA to the labeled *Phrc* probe, a clear region of protection appears, flanked on one side by a DNAse I hypersensitive band. Also, in this case, the *Cj*HrcA protected region encloses the transcriptional start site. We conclude that *Cj*HrcA binds to the *Pgro* and *Phrc* promoters by contacting DNA regions overlapping the transcription start sites, and encompassing the previously proposed CIRCE elements.

1

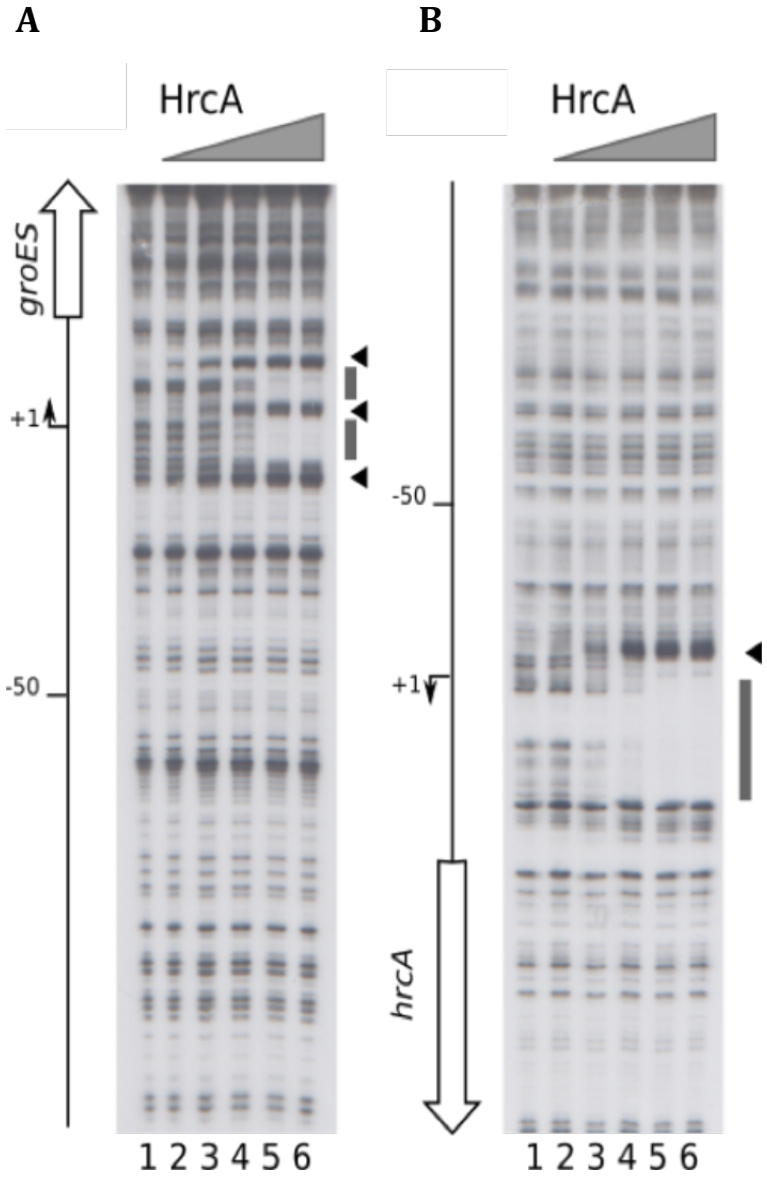

2

Pgro

```
  -40        -30        -20  V  -10        +1     V  +10        +20     V
AAGTATTGACAAAATTCATTTTTTATAGTATGATATTATCACTCTAAATTAAAGAGTGCTAAAATCAATATTTTTAA
TTCATAACTGTTTTAAGTAAAAAATATCATACTATAATAGTGAGATTTAATTTCTCACGATTTTAGTTATAAAAATT
```

Phrc

```
-40        -30        -20        -10V      +1         +10        +20
TACTTGACAAAATAACACTCAATGTTGTATAATATATCTAGCAATCAAAAAATAGAGTGCTAGATATGAAGGAAAAT
ATGAACTGTTTTATTGTGAGTTACAACATATTATATAGATCGTTAGTTTTTTATCTCACGATCTATACTTCCTTTTA
```

Figure 10: panel 1. High resolution mapping of *Cj*HrcA binding sites on heat-shock genes' promoters. DNase I footprinting assays of *Cj*HrcA on P*gro* and P*hrc* promoters. Radiolabelled DNA probes were incubated with different concentrations of recombinant *Cj*HrcA protein (0, 22, 45, 90, 180 and 360 nM *Cj*HrcA; lanes 1 to 6, respectively) at room temperature, and followed by partial DNase I digestion. In each panel, on the right the grey boxes highlight regions of DNase I protection and the black arrowheads indicate bands of DNase I hypersensitivity; while on the left bent arrows indicate the transcriptional start site and vertical open arrows depict the open reading frames; numbers refer to the positions with respect to the transcriptional start sites. **Panel 2.**: Features of *Pgro* and *Phrc* promoter sequences. For each is indicated promoter sequence, and numbers are referred to the transcriptional start site (+1). The -10 and 35 boxes are underlined bold, and the CIRCE sequences are represented in boldface. DNase I protection regions are grey highlight and the hypersensitives DNase I cut are indicated with black tick.

3.3 Characterization of the *Cj*HspR/*Cj*HrcA binding on the co-regulated promoters

Following DNase I footprinting assays described above, we have been able to identify extended *Cj*HspR binding sites on *Pgro* and *Phrc* promoters located far upstream the core promoter region, in an atypical position for a transcriptional repressor. Moreover, on the same promoters, we demonstrated the presence of a *Cj*HrcA binding site that is, instead, located within the core promoter overlapping the transcriptional start site. Notably, the distances between the *Cj*HspR and *Cj*HrcA binding sites on the *Pgro* and *Phrc* promoters are 32 and 14 bp, suggesting the possibility of direct interaction and a functional interplay between the two regulators, and potential cooperative interaction of the two repressors on these common targets.

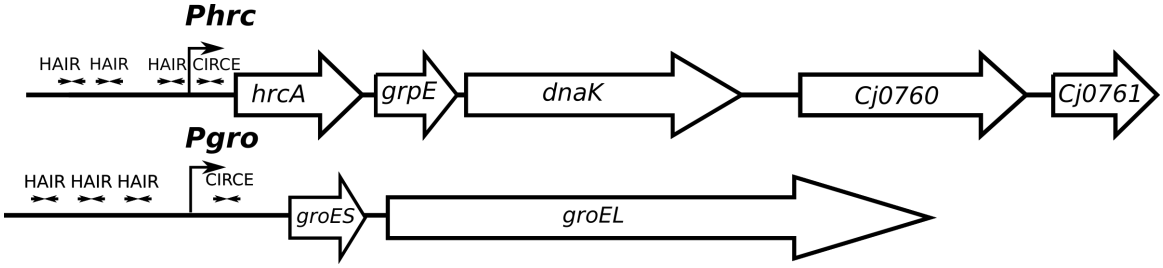

Figure 11: *hrc* and *gro* operons' schematic representation, on the promoters regions the regulatory elements are indicated.

3.3.1 *Cj*HspR and *Cj*HrcA mutual cooperative effect on DNA binding to specific operators

To study possible interactions of *Cj*HspR and *Cj*HrcA, we assayed the DNA binding activities of both proteins by carrying out DNase I footprinting experiments on *Pgro* under competitive conditions (**fig.12**). Panel A shows the results of DNA-binding assays carried out using *Cj*HspR in combination with *Cj*HrcA (lanes 7 to 12) or with a control protein (GST, lanes 1 to 6). The addition of increasing amounts of *Cj*HspR after binding of *Cj*HrcA to the labelled probe resulted in enhanced footprinting patterns compared to those obtained by incubating *Cj*HspR without *Cj*HrcA. This effect is particularly evident by comparing the intensities of all the DNase I hypersensitive bands, which appear at lower *Cj*HspR protein concentration in the presence of *Cj*HrcA. Similar result is obtained when increased concentrations of *Cj*HrcA are added to *Cj*HspR bound to the same promoter probe (**Figure 12**, **panel B**). Also in this case, the *Cj*HrcA footprinting pattern is enhanced by the incubation of the *Cj*HrcA protein with a DNA probe binding to *Cj*HspR (lanes 7 to 12), if compared to the control set (lanes 1 to 6). Consequently, we concluded that on *Pgro* co-regulated promoter and under the *in vitro* conditions used, the two regulatory proteins display a mutual cooperative mechanism of DNA binding.

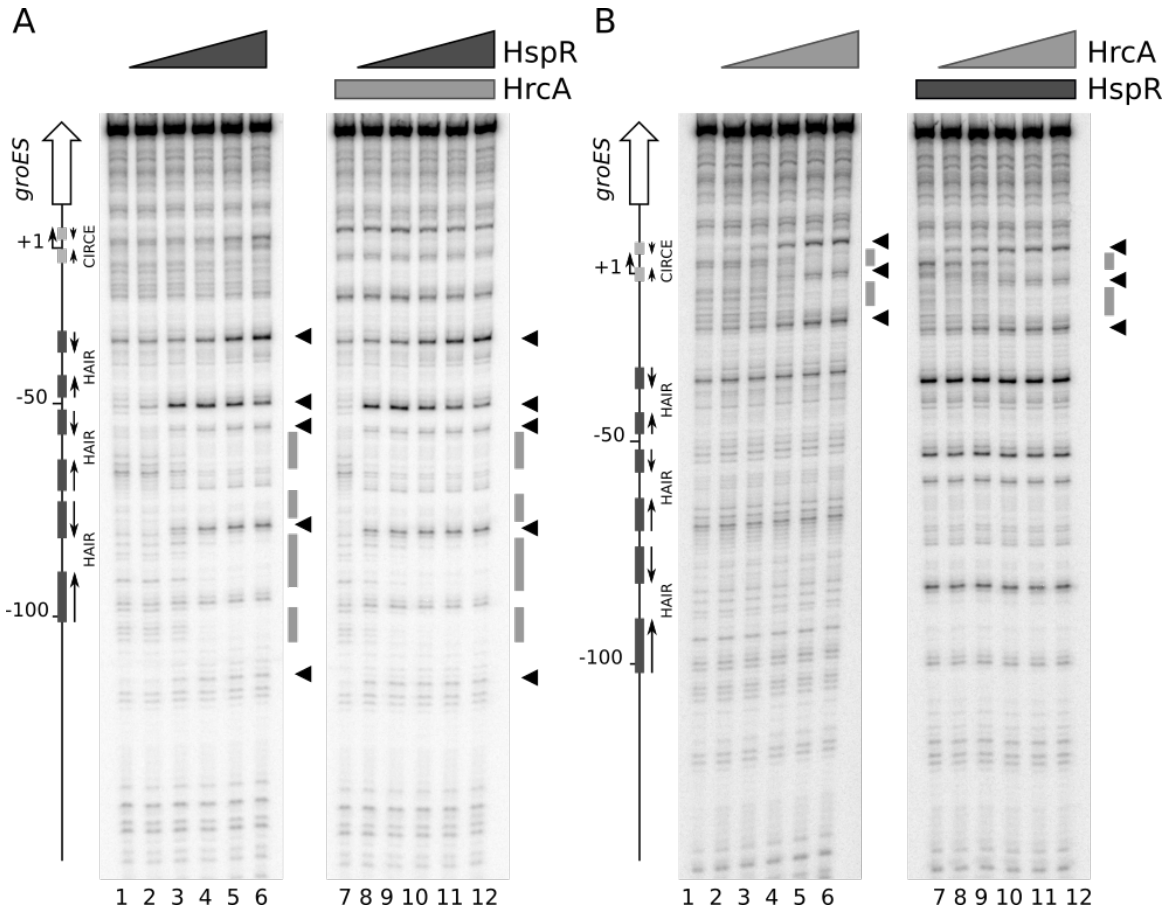

Figure 12: DNase I footprinting assays of *Cj*HspR on P*gro* (0, 22, 45, 90, 180 and 360 nM, lanes 1 to 6 and 7 to 12; panel A) with GST (360 nM, lines 1 to 6) or *Cj*HrcA (360 nM, lines 7 to 12) and *Cj*HrcA (0, 22, 45, 90, 180 and 360 nM, lanes 1 to 6 and 7 to 12; panel B) with GST (180 nM, lines 1 to 6) or *Cj*HspR (360 nM, lines 7 to 12). In each panel, on the right grey boxes highlight the regions of DNase I protection and the black arrowheads indicate bands of hypersensitivity to DNase I digestion of *Cj*HspR or *Cj*HrcA, panel A and B respectively. On the left, bent arrows indicate the transcriptional start site, vertical open arrows depict the open reading frame; numbers refer to the positions with respect to the transcriptional start sites. The HAIR and CIRCE sequences are indicated by dark and light grey boxes respectively.

3.4 Investigation of the *Cj*HspR/*Cj*HspR and *Cj*HspR/*Cj*HrcA interactions

The DNA binding experiments described above allowed to discover a complex binding architecture. More in detail, the role played by the high-affinity HAIR in promoting the *Cj*HspR binding on the flanking low-affinity site(s) may be explained by an interaction between functional units of *Cj*HspR, each of which would make contact with one DNA binding site but also with the flanking *Cj*HspR. Moreover, and as described previously, a *Cj*HspR-*Cj*HrcA interaction may be involved in the mutual cooperative effect of the two repressors. To test this hypothesis, we performed different protein-protein interaction assays.

3.4.1 *Cj*HspR and *Cj*HrcA interaction

To investigate a direct *Cj*HrcA-*Cj*HspR interaction, we performed an *in vitro* cross-linking assay with the two overexpressed and purified proteins (**fig. 13**).

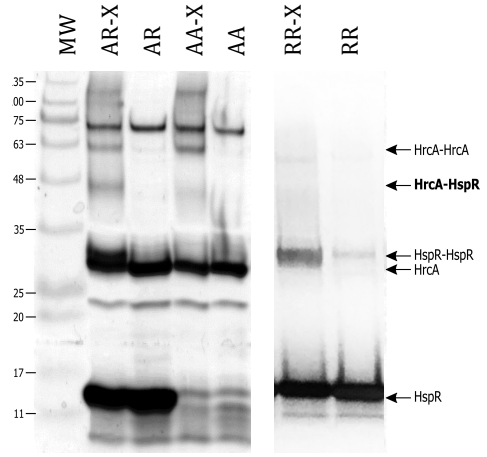

Figure 13: Cross-linking assay of CjHspR+CjHrcA, CjHrcA+CjHrcA and CjHspR+CjHspR incubated with or without glutaraldehyde. **R:** *Cj*HspR, **A:** *Cj*HrcA and **X:** glutaraldehyde.

In detail, the *Cj*HspR and *Cj*HrcA proteins were incubated separately or mixed together with a crosslinker (glutaraldehyde) and fractionated on SDS-PAGE. The results obtained indicate that both proteins could form dimers in solution. The simples containing *Cj*HspR alone (**Figure 13**, lanes labeled RR and RR-X) exhibit a significant increase of one band with an apparent molecular mass of ca. 30 kDa, only after glutaraldehyde treatment (compare lane RR with RR-X). The band observed following protein cross-link

might represent a dimeric form of the *Cj*HspR protein, considering that the molecular weight of recombinant *Cj*HspR is 15 kDa. An analogous observation is done when the crosslinker is added to the reaction containing *Cj*HrcA alone. Even if in this case the purity of the protein preparation is lower, it is possible to observe a band with apparent molecular mass of ca. 62 kDa upon addition of glutaraldehyde (**Figure 13**, lane labelled AA-X), likely representing a dimer of *Cj*HrcA (*Cj*HrcA monomer molecular weight slightly exceed ca. 30 KDa). Interestingly, the incubation of glutaraldehyde with both proteins led to the appearance of a band of ca. 46 KDa, compatible with an HrcA-HspR complex (**Figure 13**, lane AR-X). To further confirm the direct interaction between *Cj*HspR and *Cj*HrcA, we carried out a GST pulldown assay. To this aim, we expressed and purified the recombinant GST-HspR and GST-HrcA fusion proteins, which were incubated with purified recombinant His-*Cj*HspR. As a control, the same amount of purified His-*Cj*HspR was incubated with a recombinant GST protein. The GST, GST-HrcA and GST-HspR proteins were recovered after incubation employing GSH-Sepharose slurry, and the protein composition of the three samples was analysed by SDS-PAGE.

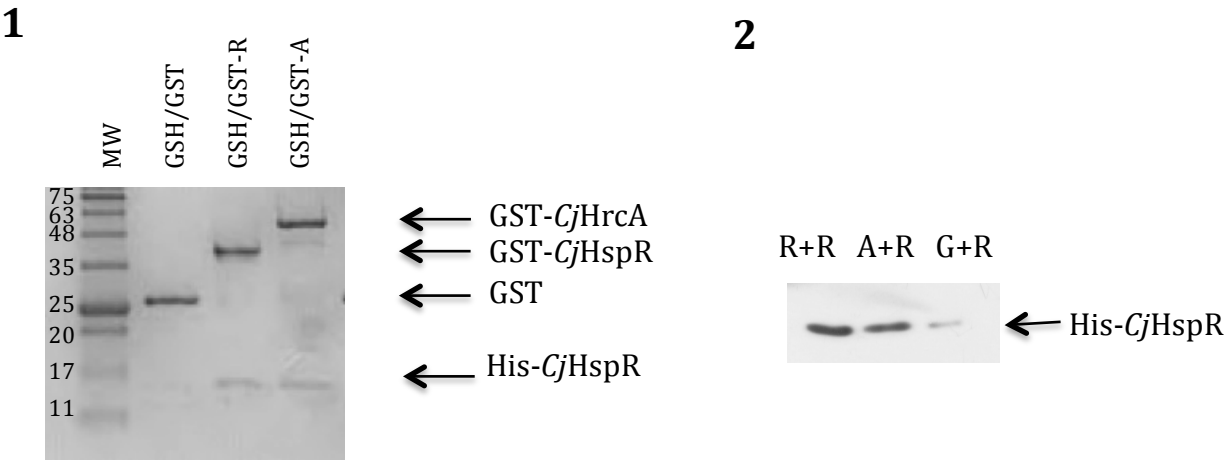

Figure 14: GST pull down assay of purified His-*Cj*HspR incubated with GST, GST-*Cj*HrcA or GST-*Cj*HspR bound to GSH-Sepharose slurry. **1.** Samples analysed with SDS-page **2.** Western blot analysis of samples stained with an anti-His antibody. **R:** *Cj*HspR, **A:** *Cj*HrcA and **G:** GST.

Using the GST-*Cj*HspR fusion protein as bait, a protein band corresponding to the expected molecular mass of *Cj*HspR was detected (**Figure 14**, panel **1**, lane R+R). The

*Cj*HspR band was absent in the control sample in which the GST bait was used (**Figure 14**, panel **1**, lane G+R). Intriguingly, also, when we used the GST-*Cj*HrcA fusion protein as bait, we detected a protein band likely corresponding to the *Cj*HspR prey (**Figure 14**, panel **1**, lane A+R). The same samples were also analysed by immunoblot assay stained with an anti-His tag antibody, able to detect only the His-tagged *Cj*HspR (**Figure 14**, panel **2**). These data strongly support the hypothesis of the propensity of *Cj*HspR to form homodimers, but also of a direct interaction between the *Cj*HrcA and *Cj*HspR repressors. Finally, the dimerization ability of the two repressors was investigated using an *in vivo* system based on the Bacterial Adenylate Cyclase Two-Hybrid System (BACTH). This assay is based on the interaction-mediated reconstitution of the recombinant adenylate-cyclase enzyme (CyaA) in *E. coli* (BTH101) strain, which is defective for adenylate-cyclase activity. It exploits the fact that the catalytic domain of CyaA from *Bordetella pertussis* consists of two distinct subunits, T25 and T18. The two subunits are inactive when physically separated, but if they are brought in close proximity to each other, the CyaA activity will be reconstituted. In the BACTH system, each one of the two enzyme fragments (T25 and T18) is fused to a polypeptide, *Cj*HrcA, or *Cj*HspR in our case. If the two analysed proteins can interact, dimerization of these hybrid proteins will take place, resulting in functional complementation between T25 and T18 subunits and in the reconstitution of the chimeric enzyme. Therefore, cAMP synthesis will occur and the cAMP will interact with the catabolite activator protein (CPR). The cAMP/CRP complex is a pleiotropic regulator of gene transcription in *E. coli*, which can turn on the expression of several resident genes, including *lacZ* that cods for the β-galactosidase (β-gal) enzymeone. Finally, the β-gal enzyme can be used as a reporter of the system, detecting the β-gal activity in a medium containing the X-gal compound, a chromogenic substrate of the enzyme. We assessed the capability of both repressors to form homo-dimers, as well as to form *Cj*HrcA-*Cj*HspR hetero-complexes. To this purpose, we set up BACTH assays, where were used the following two chimeric proteins: T25-*Cj*HspR/T18-*Cj*HspR, T25-*Cj*HrcA/T18*Cj*HrcA, T25-*Cj*HrcA/T18-*Cj*HspR or T25-*Cj*HspR/T18-*Cj*HrcA.

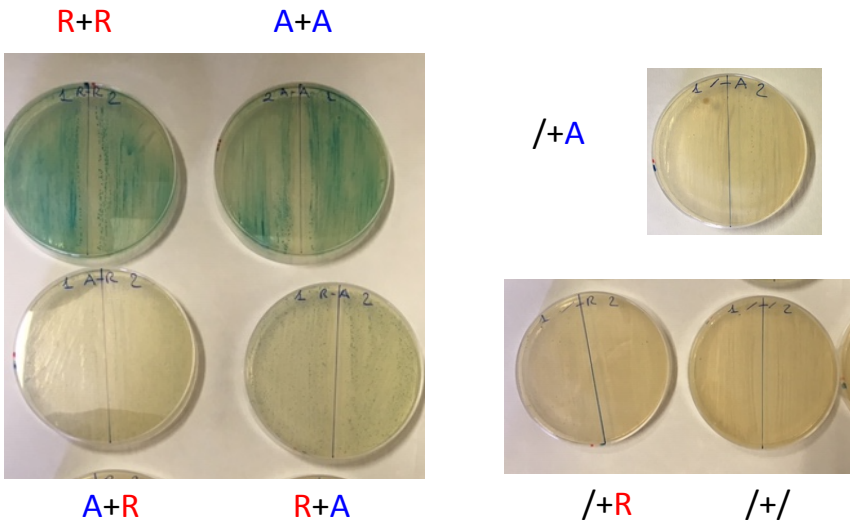

Figure 15: BACHT (Bacterial Adenylate Cyclase Two-Hybrid) System of *Cj*HspR/*Cj*HspR, *Cj*HrcA/*Cj*HrcA or *Cj*HspR/*Cj*HrcA. The β-galactosidase activity is detect growing the bacteria in LB enriched with X-gal. **R:** *Cj*HspR, **A:** *Cj*HrcA and **/:** adenylate cyclase subunits without target protein.

The results are shown in **figure 15**, and the β-gal activity is detected through the formation of insoluble blue compounds as a result of the X-gal enzyme-catalyzed hydrolysis. Our results display an evident β-gal activity in the homodimeric interaction, *Cj*HspR/*Cj*HspR (R+R), and *Cj*HrcA/*Cj*HrcA (A+A). Differently, the β-gal activity obtained starting to the hetero-complex formation, plate T25-*Cj*HrcA/T18-*Cj*HspR (A+R), and T25-*Cj*HspR/T18-*Cj*HrcA (R+A), is lower if compared with the homodimeric resulting one. However, it appears significant when compared to the three negative controls T25/T18-*Cj*HspR (/+R), T25/T18-*Cj*HrcA (/+A), and T25/T18 (/+/). Interestingly, the hetero-complex formation is more appreciable in the T25-*Cj*HspR/T18-*Cj*HrcA (R+A) sample than in the T25-*Cj*HrcA/T18-*Cj*HspR (A+R). This observation suggests peculiar gemometry of protein interaction during the formation of the *Cj*HspR-*Cj*HrcA complex. The obtained results shed light on the *Cj*HspR and *Cj*HrcA oligomeric state *in vivo* and suggested the ability of the two co-regulators to form hetero-complexes *in vivo*.

Discussion

The characterization of the heat-shock circuit in *C. jejuni* was developed starting from the information that *hspR* and *hrcA* are involved in the regulation of the heat-shock genes. Moreover, the *cis*-element associated with the two repressors, the HAIR and CIRCE motifs, were identified in the promoter regions of the most important chaperones and proteases genes. Therefore, we set up various *in vitro* binding experiments to investigate at the molecular level the HspR and HrcA interaction with different putative target promoters in *C. jejuni*. The characterization of the HspR binding on the heat-shock promoters allowed us to identify an intriguing scenario. The HspR operators are composed of multiple binding sites located in a single promoter, each one exhibiting different repressor affinity (**fig. 4**). The sequence analysis evidenced that each binding site is constituted of one HAIR motif. This evidence is in contrast with results obtained in *H. pylori* in which each operator carries only one HAIR motif, even though the binding of HspR is extended outside of the sequence motif (Pepe et al., 2018). Combined analysis of high- and low-affinity HAIR sequences alignment (**fig.5**), and DNase I footprinting assays on mutated promoter sequences (**fig. 6-7**) elucidated the specific HAIRs' features on the root of their distinct HspR affinity. Indeed, the binding hierarchy of HAIRs on a single promoter appears to be a consequence of both the IR's second emisite conservation and theHAIR specific position respect to the other HspR binding sites located on the same promoter. This evidence allowed to postulate a regulatory mechanism, where a first HspR interaction with the promoter on the high- affinity sites acts as core able to enhance the binding of other HspR functional units on the flanking binding sites. The successive bindings might stabilize the HspR interactions on the target promoters, and consolidate the repressor-promoter complex (**fig. 16**). Moreover, the described results allow speculating on the role that may have different HspR binding sites with variable repressor affinity in a cellular environment able to modulate the concentration of functional HspR. Indeed, this peculiar binding architecture may reflect in the fine regulation of the target genes expression, adapted to the specific intracellular condition.

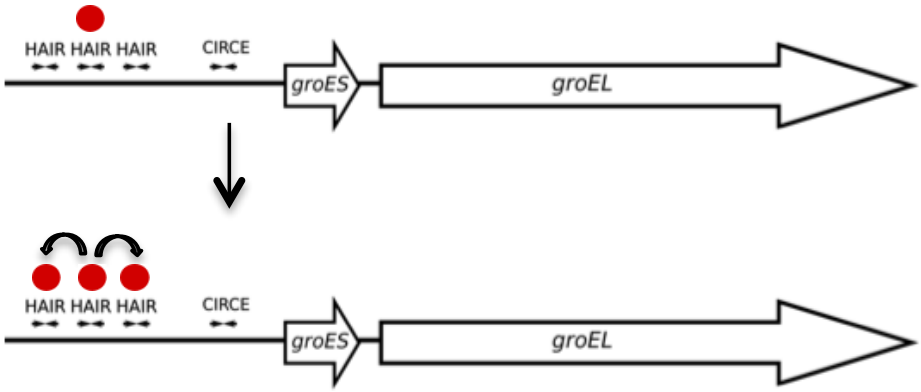

Figure 16: Schematic representation of the HspR recruitment modality on target promoter.

Although HspR alone can repress *Pcbp* and *PclpB* promoters, both HspR and HrcA regulators are necessary to repress *Pgro* and *Phrc* transcription under physiological growth conditions (Holmes et al., 2012). While HAIR-containing operators located in the core promoter region characterize the first class of promoters, the latter type owns the core HspR-operator far upstream the transcriptional start site (TSS) to an atypical position for a transcriptional repressor. A detailed *in vitro* characterization of HrcA and HspR DNA-binding, presented in this study, demonstrated that their operators are arranged in tandem on this second group of promoters, and confirmed that the CIRCE-containing operators overlap the TSS. These observations are consistent with the typical architecture for dually regulated promoters (Roncarati et al., 2017), and support the role of HrcA as HspR co-repressor also in *C. jejuni*. Different indications of interactions between the repressor units involved in this complex binding architecture are provided in the study (fig.13-14-15). These added to experimental evidence of a mutual cooperative effect of the two heat-shock repressors on the co-regulated promoters (fig.12), support a DNA-binding mechanism, where a first binding event promotes the interaction of the partner repressor (**fig.17**) and improves the formation of a stable repressive complex. Furthermore, the multiple interconnections pattern that allows between the proteins and DNA operators might stabilize the binding of the repressors, and consolidate the protein-DNA complex in our model.

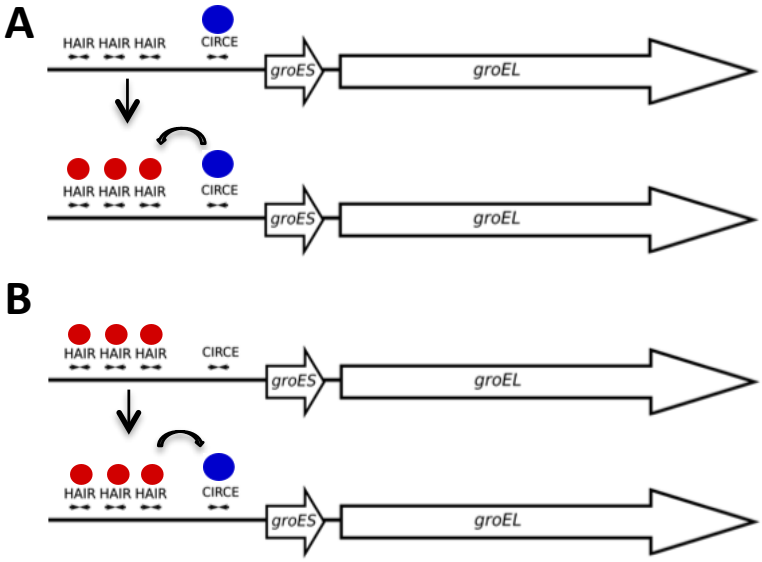

Figure 17: Model of transcriptional regulators recruitment mechanism on heat-shock promoter.

Conclusion

In this study, we started the characterization of the heat-shock regulatory circuit in *C. jejuni*. Our results support a model (**fig. 18**) in which HspR and HrcA cooperatively repress transcription of the heat-shock genes. More in detail, HspR alone controls transcription from two promoters, the *Pcpb* and the *Pclp*, thus autoregulates its expression. Differently, both the transcriptional factors HspR and HrcA regulate the majority of chaperones and proteases genes involved in the heat-shock response and the *hrcA* transcription.

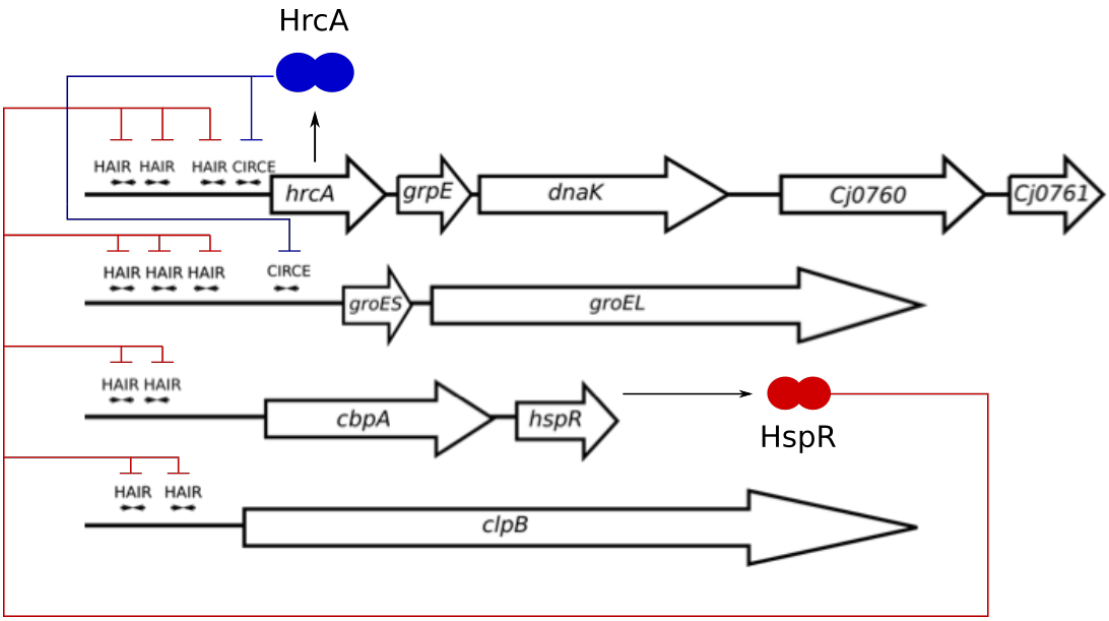

Figure 18: Regulatory circuit of HspR and HrcA on *C. jejuni*.

This work allowed to elucidate at the molecular level the repressors-promoters interactions, revealing an intricate binding site architecture, which hypothesizes a peculiar repressors-DNA interaction structure, of which a more detailed characterization would be advantageous to explain the basis of the cooperative regulation mechanism. Moreover, an investigation of the HspR and HrcA pathway by which the two transcriptional factors can sense the increase in temperature, or more generally, the heat stress condition, is indispensable to conclude the heat-shock circuit characterization.

Materials and methods

6.1.1 Bacterial strains and media

E. coli strain DH5α was used for cloning and plasmid preparation, *E. coli* strain BL21(DE3) was utilized for the overexpression of recombinant proteins, and *E. coli* strain BTH101 was used for BACTH assays. *E. coli* strains were cultured in Luria-Bertani medium. *C. jejuni* NCTC11168 cells were recovered from frozen stocks on Brucella broth agar plates containing 5% fetal calf serum, in a 9% CO_2-91% air atmosphere at 37 °C and 95% humidity in a water-jacketed incubator (Thermo Scientific). Liquid cultures were grown in Brucella Broth supplemented with 5% fetal calf serum with gentle agitation (120 rpm) under microaerophilic conditions (Oxoid). When required, kanamycin or chloramphenicol was added to final concentrations of 25 and 30 μg ml^{-1}, respectively.

Table 1: Bacterial strains used in this study.

Bacterial strain	Genotype	Reference
Escherichia coli DH5α	*supE44 ΔlacU169 (φ80 lacZΔM15) hsdR17 recA1 endA1 gyrA96 thi-1 relA1*	Hanahan, 1983
Escherichia coli BL21(DE3)	*hsdS gal (λcIts857 ind1 Sam7 nin5 lacUV5-T7 gene 1)*	Studier *et al.*, 1990
Campylobacter jejuni NCTC-11168	isolated from a case of human enteritis in the UK, wild type	Parkhill *et al.*, 2000; Gaynor et al., 2004
Escherichia coli BTH101	*cya-99, araD139, galE15, galK16, rpsL1 (Str r), hsdR2, mcrA1, mcrB1*	Battesti *et al.*, 2012

6.1.2 DNA manipulation

DNA manipulations were performed as described by Sambrook et al. (1989). All restriction and modification enzymes were used according to the manufacturers' instructions (New England Biolabs). Mini and midi scale plasmid preparations were carried out with the Nucleospin plasmid and the NucleoBond Xtra Midi plasmid purification kits, respectively (Macherey-Nagel). DNA fragments or PCR amplification

products for cloning purposes were purified from agarose gels with the NucleoSpin Gel and PCR Clean-up kit (Macherey-Nagel).

Table 2: Plasmids used in this study.

Plasmid	Description	Reference
pGEM-T-Easy	Cloning vector, Amp^r	Promega
pGEM-T-Easy-*Cj*P*cbp*	pGEM-T-Easy derivative containing a 285 bp PCR fragment (oligonucleotides *Cj*P*cbp*-F and *Cj*P*cbp*-R) that encompassing the *htrA-cbpA* intergenic region and the 5' parts of the tow genes.	This study
pGEM-T-Easy-*Cj*P*clp*	pGEM-T-Easy derivative, containing a 198 bp PCR fragment (oligonucleotides *Cj*P*clp*-F and *Cj*P*clp*-R) that comprises the P*clp* promoter.	This study
pGEM-T-Easy-*Cj*P*gro*	pGEM-T-Easy derivative carrying a 261 bp PCR fragment (oligonucleotides *Cj*P*gro*-F and *Cj*P*gro*-R) that encompassing the P*gro* promoter.	This study
pGEM-T-Easy-*Cj*P*hrc*	pGEM-T-Easy derivative containing a 421 bp PCR fragment (oligonucleotides *Cj*P*hrc*-F and *Cj*P*hrc*-R) that comprises the P*hrc* promoter.	This study
pGEM-T-Easy-*Cj*P*cbp*WT	pGEM-T-Easy derivative, containing a 89 bp fragment deriving from ssDNA *Cj*P*cbp*WT-F and *Cj*P*cbp*WT-R annealing.	This study
pGEM-T-Easy-*Cj*P*cbp*MHL	pGEM-T-Easy derivative, containing a 89 bp fragment deriving from ssDNA *Cj*P*cbp*MHL-F and *Cj*P*cbp*MHL-R annealing.	This study
pGEM-T-Easy-*Cj*P*cbp*MHR	pGEM-T-Easy derivative, containing a 89 bp fragment deriving from ssDNA *Cj*P*cbp*MHR-F and *Cj*P*cbp*MHR-R annealing.	This study
pGEM-T-Easy-*Cj*P*cbp*MH	pGEM-T-Easy derivative, containing a 89 bp fragment deriving from ssDNA *Cj*P*cbp*MH-F and *Cj*P*cbp*MH-R annealing.	This study
pGEM-T-Easy-*Cj*P*gro*WT	pGEM-T-Easy derivative containing a 169 bp PCR fragment obtained from the annealing and amplification of the ssDNA *Cj*P*gro*WT-F and *Cj*P*gro*WT-R.	This study
pGEM-T-Easy-*Cj*P*gro*MHL	pGEM-T-Easy derivative containing a 169 bp PCR fragment obtained from the annealing and amplification of the	This study

	ssDNA *Cj*P*gro*MHL-F and *Cj*P*gro*MHL-R.	
pGEM-T-Easy-*Cj*P*gro*MHR	pGEM-T-Easy derivative containing a 169 bp PCR fragment obtained from the annealing and amplification of the ssDNA *Cj*P*gro*MHR-F and *Cj*P*gro*MHR-R.	This study
pGEM-T-Easy-*Cj*P*gro*MH	pGEM-T-Easy derivative containing a 169 bp PCR fragment obtained from the annealing and amplification of the ssDNA *Cj*P*gro*MH-F and *Cj*P*gro*MH-R.	This study
pGEM-T-Easy-*Cj*P*gro*MM	pGEM-T-Easy derivative containing a 169 bp PCR fragment obtained from the annealing and amplification of the ssDNA *Cj*P*gro*MM-F and *Cj*P*gro*MM-R.	This study
pGEM-T-Easy-*Cj*P*gro*ML	pGEM-T-Easy derivative containing a 169 bp PCR fragment obtained from the annealing and amplification of the ssDNA *Cj*P*gro*ML-F and *Cj*P*gro*ML-R.	This study
pET15b	Expression vector, allowing N-terminal histidine-tag gene fusion; Amp^r	Novagen
pET15b-*hrcA*	pET15b derivative containing the *hrcA* coding sequence amplified by PCR with oligonucleotides *Cjhrc*A15b-F and *Cjhrc*A15b-R on chromosomal DNA of *C. jejuni*, digested with restriction enzymes NdeI and XhoI and ligated to pET15b.	This study
pET15b-*hspR*	pET15b derivative containing the *hspR* coding sequence amplified by PCR with oligonucleotides *CjhspR*15b-F and *CjhspR*15b-R on chromosomal DNA of *C. jejuni*, digested with restriction enzymes NdeI and XhoI and ligated to pET15b.	This study
pGEX-$_{NN}$	Expression vector, allows N-terminal GST gene fusion; Amp^r.	Novagen
pGEX-$_{NN}$-*hrcA*	pGEX-$_{NN}$ derivative containing the *hrcA* coding sequence excised from pET15b-*hrcA* by NdeI/XhoI.	This study
pGEX-$_{NN}$-*hspR*	pGEX-$_{NN}$ derivative carryng the *hspR* gene excised from pET15b-*hspR* by NdeI/XhoI.	This study
pUT18C	Expression vector, allows N-terminal T18 gene fusion; Amp^r.	Battesti A, et al., 2012
pUT18C-*hrcA*	pUT18C derivative carrying the *hrcA* coding sequence amplified by PCR (oligonucleotides *CjhrcA*-F and *CjhrcA*-R) and digested BamHI/KpnI.	This study
pUT18C-*hspR*	pUT18C derivative containing the *hspR* coding sequence amplified by PCR with oligonucleotides *CjhspR*-F and *CjhspR*-R,	This study

	digested with BamHI and KpnI.	
pKT25	Expression vector, allows N-terminal T25 gene fusion; Km^r.	Battesti A, et al., 2012
pKT25-*hrcA*	pKT25 derivative containing the *hrcA* coding sequence, PCR amplified (oligonucleotides *Cjhrc*A-F and *Cjhrc*A-R), digested BamHI/KpnI.	This study
pKT25-*hspR*	pKT25 derivative carrying the *hspR* coding sequence amplified by PCR (oligonucleotides *Cjhsp*R-F and *Cjhsp*R-R) and digested with restriction enzymes BamHI and KpnI.	This study

Table 3. Oligonucleotides used in this study.

Oligonucleotide	Sequence (5'-3')[a]	Restriction recognition site
*Cj*up*hrcA*-F	ATGCGGCCGCGCTTCCATGGGTGTGCG	NotI
*Cj*up*hrcA*-R	ATGGATCCCGAAGCAGGTATGCAAAGG	BamHI
*Cj*down*hrcA*-F	ATGGATCCGAAGGTTTTATGGGGCTTAAG	BamHI
*Cj*down*hrcA*-R	ACCTCGAGGCTACACTAACTTTGGTTGGGC	XhoI
*Cj*up*hspR*-F	ATGCGGCCGCGGACGCTCAAGAGGGGG	NotI
*Cj*up*hspR*-R	ACGGATCCGGTTCATCATAATGCTGTTCC	BamHI
*Cj*down*hspR*-F	CTGGATCCGCGGCTAGTAAAGCCGTTG	BamHI
*Cj*down*hspR*-R	GACTCGAGGTGCTGAAATTAAACTGGTAAAAAG G	XhoI
*Cj*Δ*hrcA*-F	GCACAAGATAGAAGTGTGATAGGTAAACC	
*Cj*Δ*hrcA*-R	GGATTACTTTGCTCTCGCCG	
*Cj*Δ*hspR*-F	GATCTCTTTGGAGGAGGCTTTGG	
*Cj*Δ*hspR*-R	AGCACCTGCTATAAAAGCACCC	
*Cjhrc*A15b-F	CCGCATATGATGAAAAGTCGAGATAAAAAGG	NdeI
*Cjhrc*A15b-R	GCGCTCGAGTCACGCCGCCTCCTTTATATATTG	XhoI
*Cjhsp*R15b-F	CCGCATATGGAACAGCATTATGATGAACC	NdeI
*Cjhsp*R15b-R	CGGCTCGAGTTATTTTTTCTCATAAAAAATCAA ATCAAAGC	XhoI
*Cj*P*cbp*-F	GGATCCCTTGCAGCAAATAAAGCACTTGCTAAAC	BamHI
*Cj*P*cbp*-R	CTCGAGGCTAACTCCAAGAGTTTCGTATAAACTA TTC	XhoI
*Cj*P*clp*-F	GGATCCGCATATTATCAGTTAAAAAATCTTGTA TATTTGCC	BamHI
*Cj*P*clp*-R	CTCGAGGATATTCAAAGTATAGAAGAATTAAAC AAGGC	XhoI
*Cj*P*gro*-F	GGATCCGCACAACAACAAAAGCTACAATGCC	BamHI
*Cj*P*gro*-R	CTCGAGCGCGTTTAACTAGAACACGCTTTCCTAA AGG	XhoI
*Cj*P*hrc*-F	GGATCCGAAGGAAGAAGAATGTATATTTCTATC AATGG	BamHI

*Cj*P*hrc*-R	CTCGAGCCAATAGGTGCATTATCCAAAAGATAAG	XhoI
CjhrcA-F	GCGGGATCCGATGATGAAAAGTCGAGATAAAAAGG	BamHI
CjhrcA-R	CGCGGTACCTCACGCCGCCTCCTTTATATATTG	KpnI
CjhspR-F	GCGGGATCCGATGGAACAGCATTATGATGAACC	BamHI
CjhspR-R	CGCGGTACCTTATTTTTTCTCATAAAAAATCAAATCAAAGC	KpnI
*Cj*P*cbp*WT-F	TAAATAAAACCTTGAGTGATAAAAATTTATAAAACTTGATTGACTTAGGCTAAAGTTTATGTTATAATTTAATCCTCTATATAATCAAA	
*Cj*P*cbp*WT-R	TTGATTATATAGAGGATTAAATTATAACATAAACTTTAGCCTAAGTCAATCAAGTTTTATAAATTTTTATCACTCAAGGTTTTATTTAA	
*Cj*P*cbp*MHL-F	TAAATAAAACCTTGAGTGATAAAAATTTATAAAAGAACTAAGACTTAGGCTAAAGTTTATGTTATAATTTAATCCTCTATATAATCAAA	
*Cj*P*cbp*MHL-R	TTGATTATATAGAGGATTAAATTATAACATAAACTTTAGCCTAAGTCTTAGTTGTTTTATAAATTTTTATCACTCAAGGTTTTATTTAA	
*Cj*P*cbp*MHR-F	TAAATAAAACCTTGAGTGATAAAAATTTATAAAACTTGATTGACTTAGCGATTTCTTTATGTTATAATTTAATCCTCTATATAATCAAA	
*Cj*P*cbp*MHR-R	TTGATTATATAGAGGATTAAATTATAACATAAAGAAATCGCTAAGTCAATCAAGTTTTATAAATTTTTATCACTCAAGGTTTTATTTAA	
*Cj*P*cbp*MH-F	TAAATAAAACCTTGAGTGATAAAAATTTATAAAAGAACTAAGACTTAGCGATTTCTTTATGTTATAATTTAATCCTCTATATAATCAAA	
*Cj*P*cbp*MH-R	TTGATTATATAGAGGATTAAATTATAACATAAAGAAATCGCTAAGTCTTAGTTGTTTTATAAATTTTTATCACTCAAGGTTTTATTTAA	
*Cj*P*gro*WT-F	AAAATCTTTTTCATTTTTATCCTTTAGTTTATTTTATAAAATAACTTTAGTCTATAAAACTAAACTTTTATAAATATTTTAATTTAAAGTATTGACAAAA	
*Cj*P*gro*WT-R	CCATCCTTAAAAATATTGATTTTAGCACTCTTTAATTTAGAGTGATAATATCATACTATAAAAAATGAATTTTGTCAATACTTTAAATTAAAATATTTATAAAAG	
*Cj*P*gro*MHL-F	AAAATCTTTTTCATTTTTATCCTTTAGTTTATTTTATAAAATAAGAAATCACTATAAAACTAAACTTTTATAAATATTTTAATTTAAAGTATTGACAAAA	
*Cj*P*gro*MHL-R	CCATCCTTAAAAATATTGATTTTAGCACTCTTTAATTTAGAGTGATAATATCATACTATAAAAAATGAATTTTGTCAATACTTTAAATTAAAATATTTATAAAAG	
*Cj*P*gro*MHR-F	AAAATCTTTTTCATTTTTATCCTTTAGTTTATTTTATAAAATAACTTTAGTCTATAAATGATTTCTT	

	TTATAAATATTTTAATTTAAAGTATTGACAAAA	
*Cj*P*gro*MHR-R	CCATCCTTAAAAATATTGATTTTAGCACTCTTTA ATTTAGAGTGATAATATCATACTATAAAAAATG AATTTTGTCAATACTTTAAATTAAAATATTTAT AAAAG	
*Cj*P*gro*MH-F	AAAATCTTTTTCATTTTTATCCTTTAGTTTATTT TATAAAATAAGAAATCACTATAAATGATTTCTT TTATAAATATTTTAATTTAAAGTATTGACAAAA	
*Cj*P*gro*MH-R	CCATCCTTAAAAATATTGATTTTAGCACTCTTTA ATTTAGAGTGATAATATCATACTATAAAAAATG AATTTTGTCAATACTTTAAATTAAAATATTTAT AAAAG	
*Cj*P*gro*MM-F	AAAATCTTTTTCATTTTTATCGAAATCATTATT TTTATTTTAAACTTTAGTCTATAAAACTAAACT TTTATAAATATTTTAATTTAAAGTATTGACAAA A	
*Cj*P*gro*MM-R	CCATCCTTAAAAATATTGATTTTAGCACTCTTTA ATTTAGAGTGATAATATCATACTATAAAAAATG AATTTTGTCAATACTTTAAATTAAAATATTTAT AAAAG	
*Cj*P*gro*ML-F	AAAATCTTTTTCATTTTTATCCTTTAGTTTATTT TATAAAATAACTTTAGTCTATAAAACTAAACTT TATATTTAATTTTAAAAATTTGTATTGACAAA	
*Cj*P*gro*ML-R	CCATCCTTAAAAATATTGATTTTAGCACTCTTTA ATTTAGAGTGATAATATCATACTATAAAAAATG AATTTTGTCAATAGAAATTTTTAAAATTAAATA TAAAG	

[a] Restriction sites added for cloning purposes are underlined.

6.1.2.1 Mutant DNA fragments construction

The DNA fragments *CjPcbp*WT, *CjPcbp*MHL, *CjPcbp*MHR, and *CjPcbp*MH are obtained from the ssDNA sequences *CjPcbp*WT-F and *CjPcbp*WT-R, *CjPcbp*MHL-F and *CjPcbp*MHL-R, *CjPcbp*MHR-F and *CjPcbp*MHR-R, and *CjPcbp*MH-F and *CjPcbp*MH-R (**table 3**). The couples of complementary ssDNA are mixed and boiled to 100 °C for 10 min, and gradually chilled to room temperature, to obtain dsDNA. Finally, dsDNA are purified from agarose gel. Differently, the DNA fragments *CjPgro*WT, *CjPgro*MHL, *CjPgro*MHR, *CjPgro*MH, *CjPgro*MM, and *CjPgro*ML are obtained starting from *CjPgro*WT-F and *CjPgro*WT-R, *CjPgro*MHL-F and *CjPgro*MHL-R, *CjPgro*MHR-F and *CjPgro*MHR-R, *CjPgro*MH-F and *CjPgro*MH-R, *CjPgro*MM-F and *CjPgro*MM-R, and *CjPgro*ML-F and *CjPgro*ML-R (**table 3**). The couples of ssDNA are used as primers and template in a PCR reaction to obtain the whole dsDNA fragments.

6.1.3 RNA isolation

Bacterial cells were gently harvested pipetting 10 ml of liquid cultures into a 15 ml tube containing 1.25 ml of ice-cold EtOH/Phenol stop solution (5% water-saturated phenol pH 4.5 in ethanol). Cells were spun down at 4000 rpm for 10 min at 4 °C; then, bacterial pellets were resuspended in 800 µl of lysis buffer (10 mM Tris-HCl pH 8.0, 1 mM EDTA pH 8.0, 0.5 mg/ml lysozyme) and transferred in 2 ml microfuge tubes. Samples were treated with 80 µl of 10% SDS, placed in a water bath at 65 °C for 2 min before the addition of 88 µl of 1 M NaOAc pH 5.2, and 1 ml of water-saturated phenol pH 4.5. The tubes were incubated in a 65 °C water bath for 6 min, inverting 6-10 times every 40 s, then chilled on ice and centrifuged at max speed (14000 rpm) for 10 min at 4 °C. The aqueous layer was transferred to a fresh 2 ml microfuge tube, extracted with 1 ml of chloroform and divided into two 1.5 ml microfuge tubes containing 1/10 volume of 3 M NaOAc pH 5.2 and 2 volumes of cold 100% EtOH for RNA precipitation. Samples were stored at –20 °C. Prior to use, an aliquot of each RNA sample was collected by centrifugation, quantified, and loaded on a 1% agarose gel to assess RNA purity and integrity.

6.1.4 Primer extension assays

The oligonucleotides used for primer extension reactions are listed in **Table 3**. The primer (5 pmol) was 5'-end-labeled using 6 pmol [γ-32P]-ATP (Perkin Elmer) with T4 polynucleotide kinase (NEB) at 37 °C for 45 min. Unincorporated radiolabelled nucleotides were removed with a G-25 microspin column (GE Healthcare). Labeled primer (0.1 pmol) was then added to a mix of 12 µg of total RNA, 2 µl of 2 mM dNTPs and 2 µl of 5X AMV reverse transcriptase buffer (Promega) an MQ water to a final volume of 9.5 µl. The reaction mixture was incubated at 100 °C for 3 min and cooled to 42°C before adding of 5 U of AMV reverse transcriptase (Promega). cDNA synthesis was carried at 42°C for 60 min. Lather, samples were incubated with 1 µl of RNase A (10 mg/ml) for 10 min at room temperature to remove RNA, extracted once with an equal volume of phenol–chloroform (1:1), then ethanol precipitated and resuspended in 5 µl of formamide loading buffer (99% formamide, 0.1% bromophenol blue, 10 mM EDTA pH 8.0). After denaturation at 100 °C for 3 min, samples were subjected to

electrophoresis on denaturing (6 M urea) 6% polyacrylamide gels in TBE buffer (90 mM Tris, 90 mM boric acid, 2.5 mM EDTA; pH 8.0), dried and autoradiographed.

6.1.5 Overexpression and purification of recombinant proteins

His_6-tagged recombinant HrcA and HspR proteins were overexpressed in *E. coli* BL21 (DE3) transformed with the plasmids pET15b-*hrcA* and pET15b-*hspR* (**Table 2**), respectively. Overnight bacterial cultures were diluted 1:100 in fresh LB medium and grown to an optical density at 600 nm of 0.6. Protein overexpression was induced by addition of 0.4 mM isopropyl-β-D-thiogalactopyranoside (IPTG) and carried out for 20 h at 20 °C. Bacterial pellets were stored at -80 °C. In the case of His-HrcA purification, cells deriving from 500 ml cultures were resuspended in 15 ml of lysis buffer A (50 mM NaH_2PO_4, pH 8.0; 300 mM NaCl; 10 mM imidazole; 10% glycerol; 5mM TCEP; 0.5% Triton X-100) with 1 mg/ml of lysozyme and incubated for 1 h at 4 °C. Bacterial cells were further lysed by sonication. The soluble protein fraction was incubated with 500 µl of pre-equilibrated 50% Ni^{2+}-NTA resin (Qiagen, Inc.) for 1 h at 4 °C on a tilt-roll apparatus. Samples were washed five times with 5 ml of lysis buffer A and then four times with 5 ml of wash buffer A (50 mM NaH_2PO_4, pH 8.0; 300 mM NaCl; 20 mM imidazole; 10% glycerol; 5 mM TCEP). His-HrcA was eluted five times with one volume of elution buffer A (50 mM NaH_2PO_4, pH8.0; 300 mM NaCl; 250 mM imidazole; 10% glycerol; 5 mM TCEP). 3 kDa MWCO Centricon ultra-filtration units (Millipore) were used to concentrate the protein and exchange the buffer to 10 mM Tris-HCl, pH 8.0; 300 mM NaCl; 10% glycerol; 5 mM TCEP; 0.05% NP-40 [igepal]. Purified His-HrcA was stored in aliquots at -80 °C. In regard to His-HspR purification, bacterial cells from 200 ml cultures were resuspended in 10 ml of lysis buffer R (50 mM NaH_2PO_4, pH 7.5; 300 mM NaCl; 10 mM imidazole; 10% glycerol; 1.5 mM PMSF) containing 1 mg/ml lysozyme, incubated for 1 h at 4 °C and then sonicated. The soluble protein fraction was incubated with 500 µl of pre-equilibrated 50% Ni^{2+}-NTA (Qiagen, Inc.) for 1 h at 4 °C on a tilt-roll apparatus. Nonspecific bounded proteins were removed by washing the resin five times with lysis buffer R and then four times with wash buffer R (50 mM NaH_2PO_4, pH 7.5; 300 mM NaCL; 20 mM imidazole; 10% glycerol). His-HspR was eluted by seven washing

steps with one volume elution buffer R (50 mM NaH_2PO_4, pH 7.5; 300 mM NaCl; 250 mM imidazole; 10% glycerol). Finally, the recombinant protein was dialyzed against two changes of footprinting buffer (50 mM Tris-HCl, pH 8.0; 300 mM NaCl; 10% glycerol; 1mM DTT; 0.05% NP-40 [igepal]) and stored in aliquots at -80 °C.

6.1.6 DNase I footprinting

DNA radiolabeled probes (*Cj*P*cbp*, *Cj*P*clp*, *Cj*P*gro,* and *Cj*P*hrc*; *CjPcbp*WT, *CjPcbp*MHL, *CjPcbp*MHR, and *CjPcbp*MH or *CjPgro*WT, *CjPgro*MHL, *CjPgro*MHR, *CjPgro*MH, *CjPgro*MM, and *CjPgro*ML) used for footprinting experiments were obtained by labelling with [γ^{32}P]ATP and T4 polynucleotide kinase the 5'-end of pGEM-T-Easy-*Cj*P*cbp*, pGEM-T-Easy-*Cj*P*clp*, pGEM-T-Easy-*Cj*P*gro*, pGEM-T-Easy-*Cj*P*hrc*, pGEM-T-Easy-*CjPcbp*WT, pGEM-T-Easy-*CjPcbp*MHL, pGEM-T-Easy-*CjPcbp*MHR, pGEM-T-Easy-*CjPcbp*MH, pGEM-T-Easy-*CjPgro*WT, pGEM-T-Easy-*CjPgro*MHL, pGEM-T-Easy-*CjPgro*MHR, pGEM-T-Easy-*CjPgro*MH, pGEM-T-Easy-*CjPgro*MM and pGEM-T-Easy-*CjPgro*ML (Tabel 2), previously NdeI or NcoI digested. DNA fragments corresponding to the target promoter regions were excised with second digestion with NcoI or NdeI and gel purified. DNA and recombinant proteins were incubated for 15 min at room temperature in a 50 µl reaction volume containing 1X footprinting buffer (1X FPB: 5 mM Tris-HCl, pH 8.0; 60 mM NaCl; 5 mM KCl; 5 mM $MgCl_2$; 0.2 mM DTT; 0.01% NP-40 [igepal] and 10% glycerol) and 4 ng/µl of sonicated salmon sperm DNA as nonspecific competitor. Then, 0.066 units of DNase I in 1X FPB containing 5 mM $CaCl_2$ were added at the mixture, and the reaction was incubated at room temperature for 75 s. The digestion was stopped adding 140 µl of DNase I stop buffer (192 mM NaOAc, pH 5.2; 32 mM EDTA; 0.14% SDS; 64 µg/µl sonicated salmon sperm DNA). The digested DNA was phenol-chloroform extracted, ethanol precipitated and resuspended in 13 µl of formamide loading buffer (95% formamide; 10 mM EDTA; 0.1% bromophenol blue). The samples were denatured for 5 min at 100 °C, chilled for 1 min on ice and subjected to 6% polyacrylamide-urea gel electrophoresis. The gel was dried and autoradiographed.

6.1.7 Cross-linking experiments

Cross-linking reactions were conducted by incubating 400 ng/µl *Cj*HrcA or/and 200 ng/µl of *Cj*HspR with 0.005% glutaraldehyde for 1 h at room temperature, in a final volume of 15 µl. The reaction was stopped adding 4 µl of SDS-loading buffer (SDS-LB) and incubating the samples for 10 min a 100 °C. The samples were analysed by SDS-PAGE and the proteins detected by silver staining.

6.1.8 GST pull-down experiments

6.1.8.1 Protein overexpression and slurry interaction

E. coli BL21 (DE3) strains were transformed with the plasmids $pGEX_{NN}$ or $pGEX_{NN}$-*hrcA* and $pGEX_{NN}$-*hspR* (**Table 2**) for the overexpression of GST or GST-tagged recombinant HrcA and HspR proteins, respectively. Overnight bacterial cultures were diluted 1:100 in fresh LB medium and grown to an optical density at 600 nm of 0.6. Protein overexpression was induced by the addition of 1 mM IPTG for GST and GST-HspR or 0.4 mM IPTG for GST-HrcA and carried out for 20 h at 20 °C. The bacterial pellets were resuspended in 1X PBS, 1% Triton X-100, 1 mg/ml of lysozyme and incubated for 1.5 h at 4 °C before sonication. The soluble protein fraction was then incubated with 100 µl of GSH-Sepharose resin (Glutathione Sepharose® 4B, GE Healthcare) for 1h at 4 °C. Samples were then washed four times with 1X PBS to remove nonspecific protein interactions and finally resuspended in 100 µl of 1X PBS. The bound GST/GSH Sepharose, GST-HspR/GSH Sepharose, and GST-HrcA/GSH Sepharose were quantified thought SDS-PAGE.

6.1.8.1 GST pull-down analysis

An equal amount of GST/GSH Sepharose, GST-HspR/GSH Sepharose or GST-HrcA/GSH Sepharose was incubated with 250 ng/µl of purified recombinant His-HspR in a final volume of 200 µl 1X FPB for 1.5 h at 4 °C. The samples were washed seven times with 1X FPB and the pulled-down proteins analysed by SDS-PAGE and Western blot assay. For

the Western blot analysis, the proteins were separated by SDS-PAGE and blotted onto a nylon (PVDF) membrane using a wet transfer apparatus (BioRad). The transfer was conducted for 1 h at 150 V in transfer buffer (48 mM Tris, 39 mM glycine, 20% methanol, 0.037% SDS). Membranes were incubated in blocking solution (5% low-fat milk in 1X PBS, 0.05% Tween-20 or 1X PBST) for 1 h at room temperature. Membranes were then rinsed three times for 5 min in 1X PBST and incubated with the primary antibody (dilution 1:5000 of mouse anti-His clone HIS.H8 monoclonal antibody, Sigma Aldrich) in 5% skim milk-1X PBST, for 1 h at room temperature. After washing three washings in PBST (1× PBS; 0.05% Tween-20), the membranes were incubated with a 1:10000 dilution of the horseradish peroxidase-conjugated α-mouse secondary antibody for 3 h at room temperature. Following three washing steps in PBST, the immunoblot was developed by pouring on the membranes a solution of 1.25 mM luminol containing 0.015% H_2O_2 and 0.068 mM p-coumaric acid. The signal was visualized by film-autoradiography.

6.1.9 Bacterial Adenylate Cyclase Two-Hybrid System (BACTH) assays

E. coli BTH101 cells co-transformed with pUT18C-*hspR*/pKT25-*hspR*, pUT18C-*hrcA*/pKT25-*hrcA,* pUT18C-*hspR*/pKT25-*hrcA,* pUT18C-*hrcA*/pKT25-*hspR*, pUT18C-*hspR*/pKT25, pUT18C-*hrcA*/pKT25 or pUT18C/pKT25 (**tab. 2**) were grown on LB agar plates added of 0.5 mM IPTG and 40 µg/ml X-gal (5-Bromo-4-Chloro-3-Indolyl β-D-Galactopyranoside) for 1 week at 25 °C.

Urease inactivation by gold-based compounds

Introduction

1.1 Urease

Urease is an enzyme catalysing the nitrogen organic's last step mineralization, which is the urea hydrolysis, to obtain ammonia and carbonate, which spontaneously decomposes to yield another molecule of ammonia and carbonic acid (Zambelli, Musiani, Benini, & Ciurli, 2011). Urea is broadly used as a fertilizer in agriculture, but the urease activity of soil bacteria determines an ammonia production with the loss of the organic nitrogen source, and a consequent pH increase that damaged the plant rooting apparatus. Moreover, many pathogenic bacteria, such as *Helicobacter*, *Proteus*, *Klebsiella*, *Pseudomonas*, and *Mycobacterium* spp. use this enzyme as an essential virulence factor (Farrugia, Macomber, & Hausinger, 2013).

1.1.1 Urease as virulence factor

The urease phenotype is widely distributed across the bacterial kingdom, and the gene clusters encoding this enzyme have been found in numerous bacterial species (Mobley, Island, & Hausinger, 1995). Among the different ureolytic bacteria, some of these are humans pathogens commonly involved in infections of urinary and gastrointestinal tracts (Burne & Chen, 2000) (Collins & D'Orazio, 1993). The pathogenesis of these bacteria is closely related to their ureolytc activity, in particular, with the pH increase and the toxicity of released ammonia. The human pathogen *H. pylori* can colonize the gastric tract, eliciting gastritis, gastroduodenal ulcers, and cancer-induced by chronic gastroduodenal infections. Although *H. pylori* is a neutrophil bacterium, it can survive in the acidic environment of the stomach, thanks to its urease activity able to neutralize the hostile acid condition by exploiting the pH increase caused by the urease mediated ammonia production. This evidence makes the urease a virulence factor crucial at the beginning of infection, and indispensable for the occurrence of subsequent host-pathogen interactions (Montecucco & Rappuoli, 2001). In *H. pylori*, the majority of the acid resistance is given by an intracellular urease; its activity is regulated by the availability of substrate, in turn, checked by the proton-gated urea channel (UreI).

Indeed, UreI is located in the bacterial inner membrane, and allows substrate entry only at low pH (5.0), when the channel is fully open (Weeks, Eskandari, Scott, & Sachs, 2000). The rapid entry of urea in *H. pylori* cells allows the massive production of urea-derived ammonia, which is extruded across the inner membrane by UreI and enables the fast neutralization of protons invading the periplasm (Scott et al., 2010). Interestingly, the urease seems also involved in the nitrogen metabolism, judgment supported by indications about the urea-derived ammonium assimilation into amino acid (Miller & Maier, 2014). Additionally to the intracellular urease, this protein is also found on the cell surface as a consequence of bacterial lysis. The extracellular enzyme supports the intracellular urease activity, quickly neutralizing the acidic micro-environment close to the *H. pylori* cells (Weeks et al., 2000). Moreover, the urease is also involved in microorganism-macrophage interactions. This evidence highlights a role for this virulence factor even during the subsequent stage of infection. More in detail, the urease mediated ammonia production can modulate phagosome pH and megasome formation, and allows the *H. pylori* survival in macrophage (Schwartz, 2006). Between the urinary tract infections, the majority of clinical cases being associated with ureolytic *Proteus*, *Klebsiella*, *Pseudomonas,* and *Staphylococcus* spp. (Mobley & Hausinger, 1989). The pathogen *P. mirabilis* owns a urea-induced urease that is found in the cytoplasm of the bacterium. During infection in the urinary tract, the expression of urease, and the subsequent ammonia production, resulting in a pH increases. The basic pH in the local environment promotes the precipitation of polyvalent ions (Mg^{2+} and Ca^{2+}), normally soluble in the urine, and the consequent formation of struvite and carbonate hydroxyapatite crystals (i.e., stone formation), respectively. Stone formation provides several benefits connected to *P. mirabilis* cells protection, but also to formation of a nutrient-rich environmental niche, tanks to blockage of urine drainage into the ureters, protection from host immune system, and ammonia toxicity to host cells with direct tissue damage (Coker, Poore, Li, & Mobley, 2000). Differently, in *M. tuberculosis*, the urease inducted ammonia production is involved in phagosome-lysosome fusion inhibition and the modulation of the phagosome pH. Moreover, the urease activity resulting ammonia is a nitrogen source for biosynthesis (Clemens, Lee, & Horwitz, 1995).

1.1.2 Urease as antibacterials target

The idea to use the urease virulence factor as a novel target for antimicrobials starts from the necessity to find new strategies in pathogen eradication, considering the widespread bacterial resistance to conventional antimicrobial agents. Different works indicated urease inhibition as a valuable tool in hindering the cascade of events that elicit the whole symptomatology of urinary infection (Kosikowska & Berlicki, 2011). Moreover, increasing antibiotic resistance compromises also the treatment of *H. pylori* infection. In this pathogen, the urease targeting approach to eradicate the bacterium appears extremely beneficial. Urease negative mutants are unable to colonize gastric epithelium (Eaton, Brooks, Morgan, & Krakowka, 1991) (Schoep et al., 2010), and urease inhibition would compromise the *H. pylori* ability to survive in the stomach acid environment and colonize the epithelium cells(Kao, Sheu, & Wu, 2016). In 2017, the World Health Organization (WHO) published the list of bacteria for which new antibiotics are urgently needed. Interestingly, ten out of the twelve antibiotic-resistant pathogens prioritized are ureolytic bacteria. Among these are *H. pylori, M. tuberculosis, C. neoformans*, and *Y. pestis*. This evidence made the urease inhibition a fascinating way to find novel antibacterials with a ureolytic-specific activity.

1.1.3 Urease structure

It is available in the literature the characterization at the molecular level of the protein architecture for ureases deriving from different bacteria species such as *Klebsiella aerogenes* (KAU) (Jabri, Carr, Hausinger, & Karplus, 1995) *Sporosarcina pasteurii* (SPU) (Stefano Benini et al., 1999) and *H. pylori* (HPU) (Ha et al., 2001), and from the plant *Canavalia ensiformis* (jack bean, JBU) (Balasubramanian & Ponnuraj, 2010). These studies illustrate that in most bacteria urease (*e. g.* KAU and SPU) is structured to obtain a trimer of trimers, each one composed of the subunits α, β and γ (Jabri et al., 1995) (Stefano Benini et al., 1999). Differently, in *H. pylori* the β and γ subunits are fused; therefore, the quaternary structure is composed of trimers of dimers, which are assembled in a tetrahedral structure harboring a total of 22 active sites (Ha et al., 2001). Finally, in JBU, the three bacterial subunits are fused in a unique polypeptide to collect a dimer to omo-trimers (Balasubramanian & Ponnuraj, 2010) (**fig.19**).

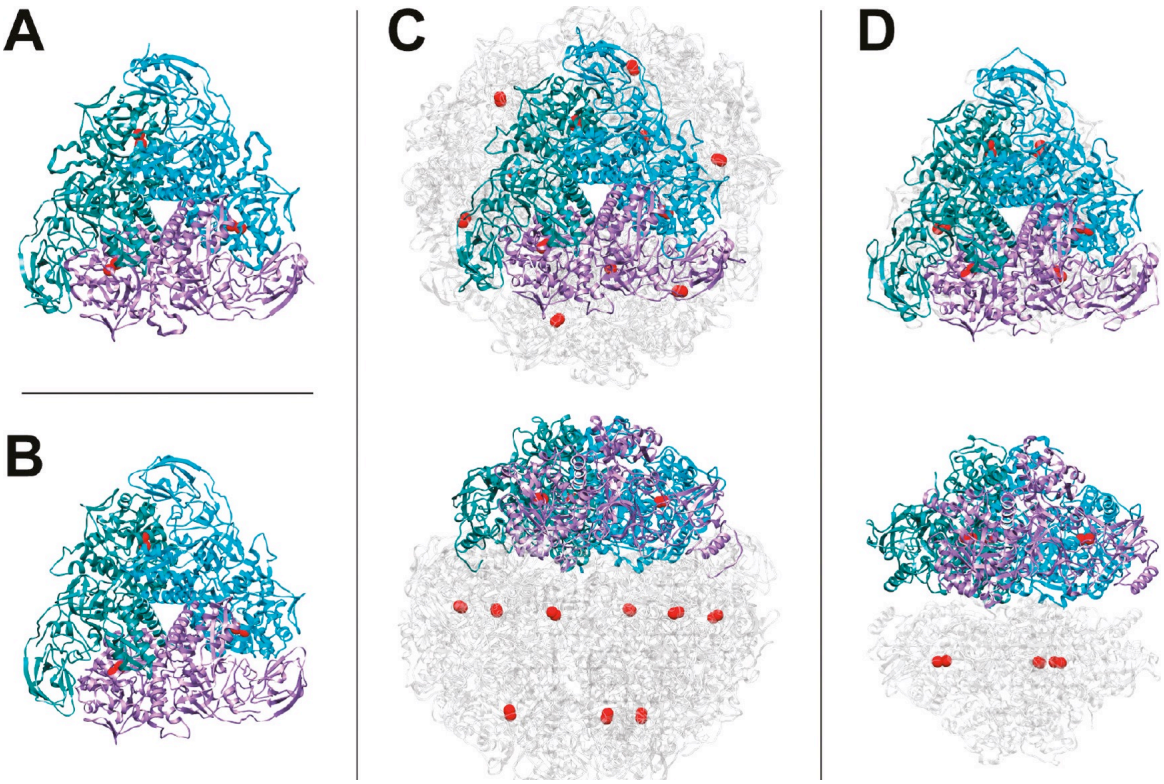

Figure 19: graphical representation of ureases from *S. pasteurii* (PDB code: 2USP), (B) *K. aerogenes* (PDB code: 1EJZ), (C) *H. pylori* (PDB code: 1E9Z) and (D) jack bean (PDB code: 3LA4). The red sphere indicates the nickel ions, while the units that produce the trimer are depicted with different colours. Reprinted with permission from (Zambelli et al., 2011). Copyright 2019 American Chemical Society.

Despite the differences in the quaternary structure of the enzyme from distinct biological sources, the catalytic site is strongly conserved among bacteria and plants. The catalytic site (**fig. 20**), is always located in the α subunits and contains two nickel ions, distant 3.5 – 3.7 Å. Each Ni^{2+} is associated with two histidine residues and connected to an oxygen atom of a carbamylated lysine. Additionally, one nickel is bound to carboxylate oxygen of aspartate, and the binding geometry is concluded by an H_20 bond to each ion and a hydroxide ion linking the two metals. Therefore, one Ni^{2+} is penta-coordinated with a distorted square-pyramidal geometry while the other Ni^{2+} is hexa-coordinated and has a distorted octahedral geometry. The tetrahedral cluster is concluded with one water hydrogen bond to constitute the binding network in the closeness of the nickel ions. The catalytic site is located in a cavity able to stabilize the intermediate and the tetrahedral transition state. Additionally, the protein possesses a helix-turn-helix (HTH) mobile flap essential for the catalytic activity, which regulates the entry of the substrate in the catalytic cavity. Because of this mobility of the flap, an essential histidine in the HTH motif swings of 5 Å between the open and closed conformations (Zambelli et al., 2011).

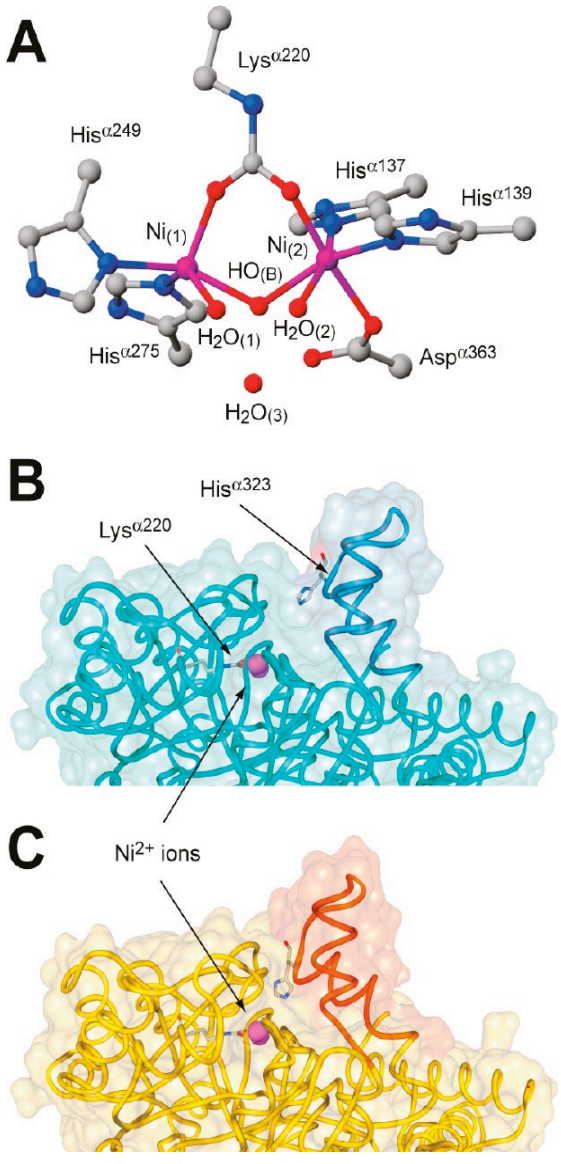

Figure 20: Coordination geometry of Ni^{2+} on the active site (**A**). The nickel is represented in purple; carbon in gray; nitrogen in blue; oxygen in red. The mobile flap is depicted in the open (**B**) and closed (**C**) conformation. In B and C Ni^{2+} ions are highlighted as purple spheres. Reprinted with permission from (Zambelli et al., 2011). Copyright 2019 American Chemical Society.

1.1.4 Urease inhibition strategy

The urease inhibitors can be divided into two families, characterized by a different inactivation mechanism. Molecules able to directly interact with the Ni^{2+} ions located in the catalytic site compose the first group. This class includes compounds as sulphite, phosphorodiamidate, thiols, phosphate, citric, hydroxamic and boric acids and fluoride (Stefano Benini et al., 1999) (Stefano Benini, Cianci, Mazzei, & Ciurli, 2014) (Ha et al., 2001) (Luca Mazzei et al., 2017). The second class of inhibitors blocks the mobility of the urease mobile-flap that plays a crucial role during the urea catalysis. Indeed compounds as the 1,4-benzoquinone and the catechol directly interact with a conserved cysteine located in the helix-turn-helix motif, and therefore interfere with the substrate entrance into the catalytic cavity (L. Mazzei, Cianci, Musiani, & Ciurli, 2016) (Luca Mazzei et al., 2017). Biochemical information demonstrates that metals act as urease inhibitors (Krajewska, 2009). Metal ions are able to react with sulfhydryl of cysteine residues. Therefore ions as Hg(II), Ag(I), and Cu(II) exert their inactivating function contacting the Cys located on the mobile-flap. In the case of Cu(II), the generation of reactive oxygen species may elicit the oxidation of functional groups with subsequent urease inactivation (Krajewska, 2008). Moreover, compounds as the 2-mercapto-ethanol can inactivate the urease by both interacting with Ni^{2+} ions and binding the Cys residue of the mobile-flap (S. Benini, Rypniewski, Wilson, Ciurli, & Mangani, 1998).

1.1.5 Urease inhibitors as potential drugs

Hydroxamic acids are considered the most widely studied group of urease inhibitors. Although the FDA approved it in 1983 to treat chronic urea-splitting urinary infections, the compound had severe aftereffects, such as teratogenicity, psychoneurological, and musculo-integumentary symptoms (Bailie et al., 1986). At the leader time, hydroxamic amino acids and their N-substituted derivatives were inspected. N-aroyl-glycine-hydroxamic acids were largely investigated with interesting results and inhibitors patented for treating urolithiasis and pyelonephritis. However, the majority of these compounds were proven as mutagenic (Munakata, Mochida, Kondo, & Suzuki, 1980). The amides of phosphoric acid are the class of urease with the highest urease inhibitory activity (Keerthisinghe & Blakeley, 1995). Nevertheless, these inhibitors exhibit low

hydrolytic stability (Pope et al., 1998). Some non-hydrolysable analogous of phosphoramidates, instead, were determined to be useful inhibitors of bacterial ureases (Vassiliou et al., 2008). Quinones are an interesting class of urease inhibitors that also shows inactivating properties toward the urease in whole cells of *H. pylori*, *K. oxytoca,* and *P. mirabilis*, tanks to the ability to pass by membranes. But their cancerogenic and cytotoxic properties make the group of compounds not suitable in medicine (Kosikowska & Berlicki, 2011). Polyphenols represent an intriguing class of molecules, which are highly bioavailable in medicinal. Although some of these exhibits only a discrete urease inactivating ability (Tanaka, Kawase, & Tani, 2004).

1.2 Gold-based drugs

Metals and metal-based compounds have been largely used as antimicrobial agents for centuries. In recent years, research into gold-based drugs for a range of human diseases has seen a revival. In the modern pharmacology, gold cyanide was first proposed as an antitubercular agent. Successively, the therapeutic features of gold complexes were widely investigated, unveiling its encouraging potentiality as an anti-arthritis, anticancer, antibacterial and anti-parasitic (Sannella et al., 2008) (Roder & Thomson, 2015) (Aguinagalde et al., 2015). The clinical practice is mainly based on the use of Au(I) and Au(III) compounds. As an example, the use of Au(I)-based phosphirine complexes and auranofin [2,3,4,6-tetra-o-acetyl-L-thio-β-D-glucopyranosato-S-(triethyl-phosphine)Au(I)] displayed antibacterial properties against gram-positive and gram-negative bacteria (Owings et al., 2016) (Fernández, Vela Gurovic, Olivera, Chopa, & Silbestri, 2014) (C. Schmidt et al., 2017). Although the antimicrobial activity of these compounds was demonstrated, their biomolecular targets and mechanisms of action in bacteria have not yet been defined. Differently, it is known that their ability to interact and inhibit the mammalian seleno-enzyme thioredoxin reductase (TrxR) is due to the formation of Au-selenol in the proximity of the active site (Bindoli et al., 2009). Concerning the Au(III)-based compounds, less information is available. Au(III)-complexes, as phosphorous dendrimers bearing iminopyridino-end groups coordinating to Au(III) ions, showed inhibition property on the growth of gram-positive and gram-negative bacteria (Mignani et al., 2017) (Warzajtis et al., 2017).

Aim of the project

Urease is an enzyme that plays a crucial role as a virulence factor in the pathogenesis of different microorganisms, like *H. pylori, M. tuberculosis, C. neoformans*, *Y. pestis*, and *P. mirabilis*. The purpose of this work is to characterize the inhibition of different Au(III)-based compounds on the urease enzyme, to investigate the potentiality of these compounds as a future antimicrobial in ureolytic bacteria. With this aim, we implement different enzymatic assays to obtain a kinetic characterization of the inhibitory activity of these Au(III)-complexes and to elucidate the mechanism at the root of their capability to inactivate the urease enzyme. The results obtained in this study are part of a published work (Luca Mazzei et al., 2019).

Results

3.1 Au(III)-based compounds' inhibition on urease activity

3.1.1 Introduction to fast and slow binding inhibition

We performed a variety of enzymatic assays to obtain information about the inhibitory effect of different Au(III)-based compounds on jack bean urease (JBU). More in detail, the following inhibition scheme is considered (**scheme 1**):

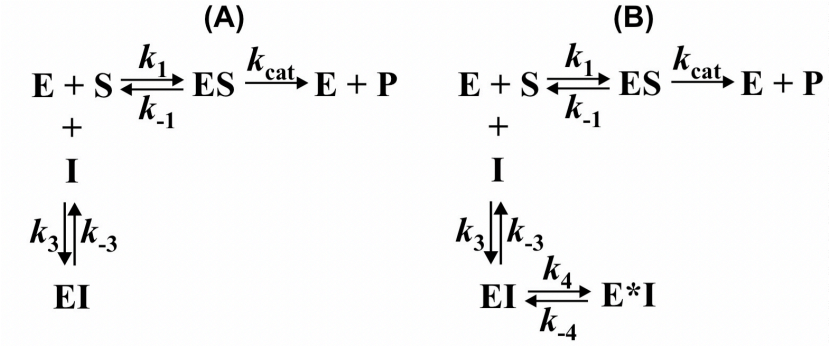

This representation allows explaining the differences between a fast- or slow-binding enzyme inhibition model. Indeed, a fast mechanism considers that the equilibrium between the free enzyme (E) and inhibitor (I) with the enzyme-inhibitor complex (EI) has association and dissociation kinetic values (k_3 and k_{-3}) of the same magnitude's order of the constants (k_1 and k_{-1}) involved in the equilibrium between the enzyme and the substrate (S) with the enzyme-substrate complex (ES). Differently, a slow-binding inhibition may be explained in two ways. In mechanism A, the EI complex is assembled in a single event that displays k_3 and k_{-3} values smaller if compared with k_1 and k_{-1}. Mechanism B involves two steps: an initial rapid formation of the EI complex governed by the k_3 and k_{-3} constants, developing in a more stable E*I complex through an isomerization step characterized by the kinetic constants k_4 and k_{-4} (John F. Morrison, 1982) (J. F. Morrison & Walsh, 1988). It is possible to discern between a fast inhibition process and a slow-binding inhibition

analysing the evolution of the substrate consumption (Δ[S]) over time (t). The Δ[S]/t curve is linear in the presence of a fast mechanism. In contrast, it exhibits a progression divided into three time-dependent phases if we consider a slow-binding mechanism. Specifically, the time-depended inhibition is composed of an initial linear phase occurring when the enzyme-inhibitor interaction has not been established, followed by a deviation from linearity as a function of time proceeding proportionally with the enzyme-inhibitor complex formation. Finally, the reaction arrives at a steady-state, representing the equilibrium of the system. Starting from the progress curves, it is possible to obtain the initial velocity of the reaction (v_i) which is the slope of the curve in the initial linear phase, and the steady-state velocity (v_s) as the slope of the last phase (John F. Morrison, 1982) (J. F. Morrison & Walsh, 1988). Differently, if we consider the two-step isomerization mechanism (scheme 1, mechanism B) the v_i derived from the EI complex formation, and the v_s is the consequence of the affinity for the final complex E*I (Copeland, 2013).

3.1.2 Au(III)-based compounds inhibit urease with a slow-binding mechanism

Based on the previously described information, we performed progress curve experiments of urea hydrolysis at increasing concentration of Au(III)-based inhibitors (**fig.21**) to monitor the substrate consumption. In our system, ammonia formation consequent to urea degradation determines a change in absorbance elicited to the pH increase.

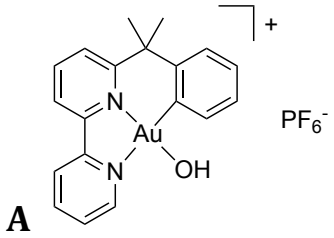

A

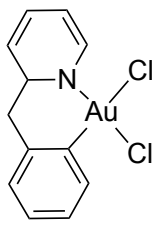

B

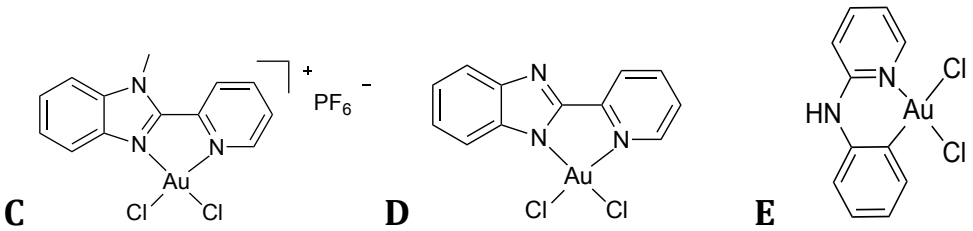

Figure 21: Schematic representation of the Au(III)-based compounds tested as urease inhibitors; (A) AuC^N^N, (B) MNW033, (C) MNW034, (D) MNW102, and (E) MNW107.

The obtained progress curves (**fig.22**) demonstrate the ability of all tested Au(III)-complexes to inhibit the urease enzyme, and exhibit a clear deviation from linearity; this indicates that the interaction between JBU with all compounds involves a slow-binding mechanism. The collected curves revealed an initial very short linear phase that evolved by an intermediate step to reach the steady-state. Unfortunately, since the initial linear phase is too brief, it was not possible to obtain precise substrate consumption curves with our equipment, and a consequent kinetic characterization of inhibition starring with this enzymatic assay. Although the reported data are not sufficient to obtain an accurate kinetic characterization of the tested inhibitors modality, any consideration is possible. Indeed, a higher inhibitor concentration is required for the A and E compounds, if compared with the C and D inhibitors, whereas an intermediate concentration is needed for the B compound. These results highlight that the formation of the E*I complex is faster for the C and D molecules and slowest in the presence of A and E.

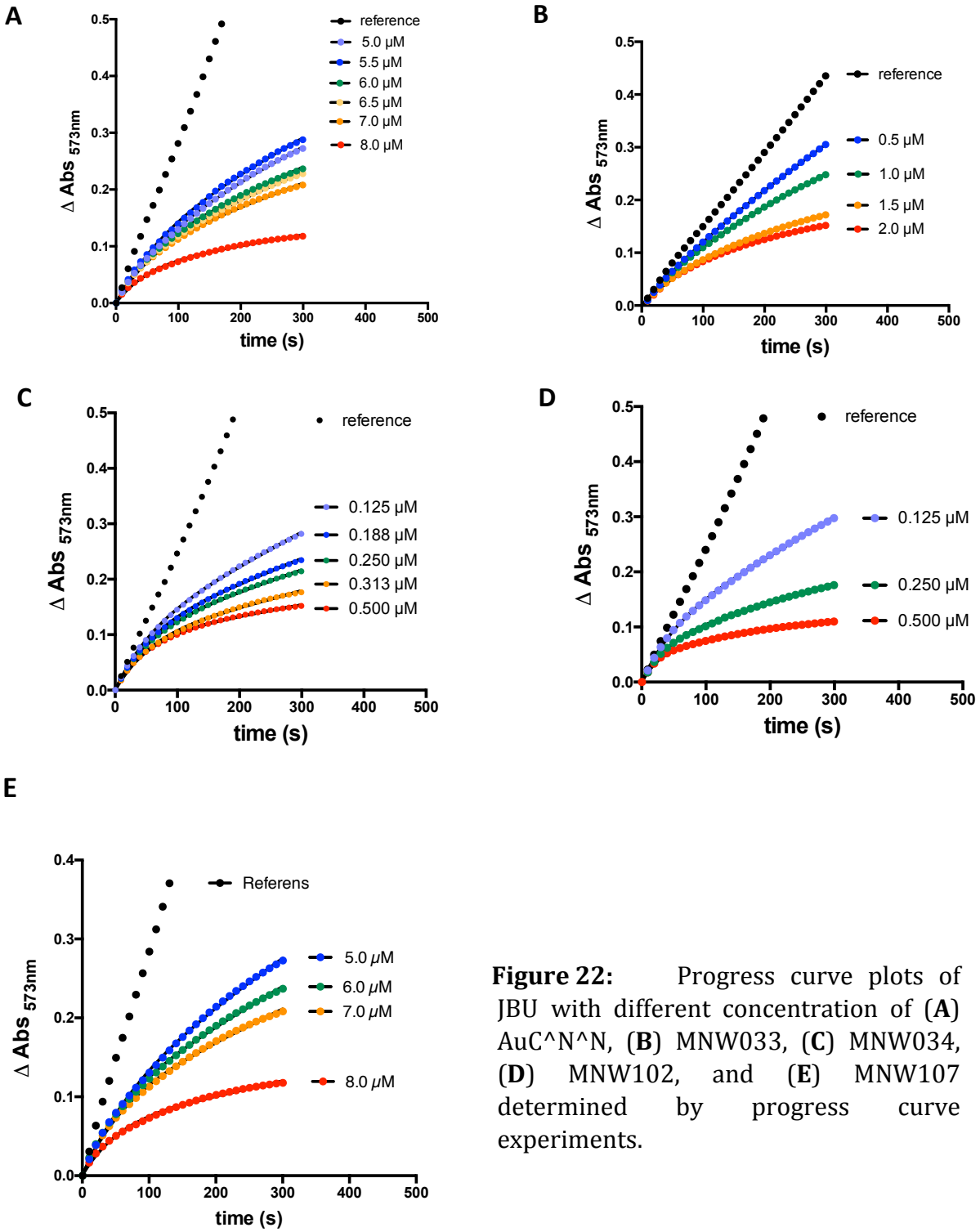

Figure 22: Progress curve plots of JBU with different concentration of (**A**) AuC^N^N, (**B**) MNW033, (**C**) MNW034, (**D**) MNW102, and (**E**) MNW107 determined by progress curve experiments.

3.1.3 Evaluation of the K_i and K_i^*

In the two-step isomerization mechanism, the apparent values of K_i (k_3/k_{-3}) and K_i^* (k_4/k_{-4}) were recovered from the concentration-response plots of the initial and finally inhibited states respectively (Copeland, 2013). Furthermore, considering the non-competitive modality proposed for these Au(III)-base inhibitors, the apparent K_i and K_i^* can be considered as the true K_i and K_i^*. The K_i of different compounds were obtained (**tab.4**), starting from the v_i values measured using the initial rate experiments. Thus the residual activity calculated as v_i/v_0 (where v_0 is the reaction velocity in the absence of inhibitor) was plotted as a function of inhibitor concentration (**fig. 23**) and fitted with the **equation 1**.

$$\frac{v_i}{v_0} = \frac{1}{1+\left([I]/K_i^{app}\right)} \qquad \textbf{Eq. 1}$$

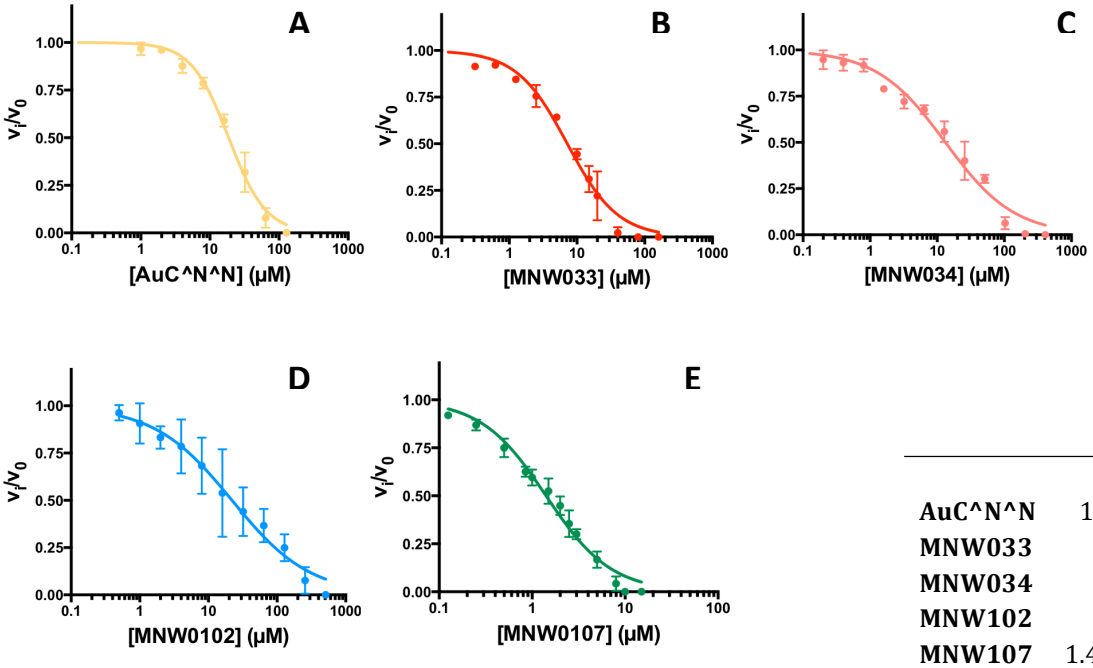

	K_i (μM)
AuC^N^N	18.6 ± 0.8
MNW033	7.2 ± 0.4
MNW034	13 ± 1
MNW102	22 ± 3
MNW107	1.41 ± 0.06

Figure 23: Concentration-response plots of the initial inhibited state of JBU with Au(III)-based compounds, (**A**) AuC^N^N, (**B**) MNW033, (**C**) MNW034, (**D**) MNW102 and (**E**) MNW107.

Table 4.: *Ki** values obtained for the Au(III)-based inhibitors with JBU.

Differently, the K_i^* was characterized by pre-incubation experiments. This assay allows to obtain the v_s that is the velocity of the reaction after a pre-incubation time, that is the time required to reach the equilibrium of the final E*I complex, spacing between 40' and 8 h. Then the residual activity in the steady-state (v_s/v_0) was used to obtain the concentration-response plots (**fig. 24**). Finally, the K_i^* values (**tab. 5**) are extracted, fitting the data with **equation 2**.

$$\frac{v_s}{v_0} = \frac{1}{1+\left([I]/K_i^{*app}\right)} \qquad \textbf{Eq. 2}$$

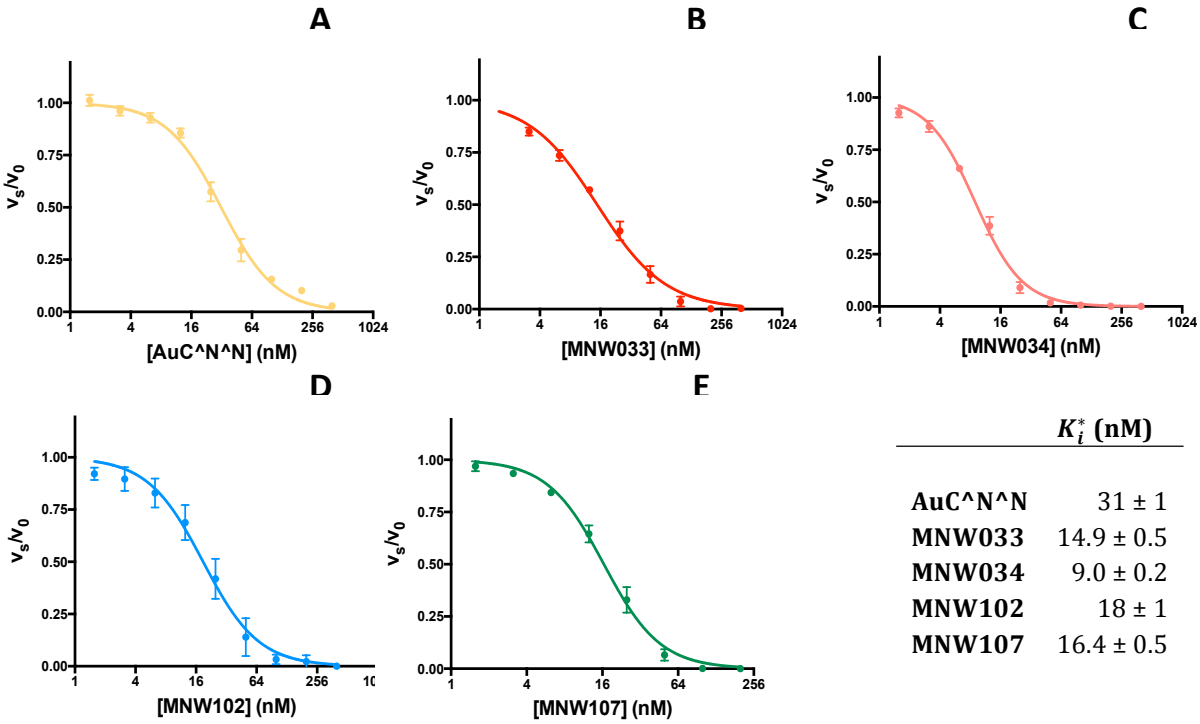

	K_i^* (nM)
AuC^N^N	31 ± 1
MNW033	14.9 ± 0.5
MNW034	9.0 ± 0.2
MNW102	18 ± 1
MNW107	16.4 ± 0.5

Figure 24: Concentration-response plots of the final inhibited state of JBU with Au(III)-based compounds, (**A**) AuC^N^N, (**B**) MNW033, (**C**) MNW034, (**D**) MNW102 and (**E**) MNW107.

Table 5: Ki values obtained for the Au(III)-based inhibitors with JBU.

Interestingly, al the tested compound show a strong inactivating ability with K_i^* values in the low nanomolar concentration range. This result highlights the marked inhibiting activity of A(III)- based compounds.

Discussion

The five Au(III)-based compounds (AuC^N^N, MNW033, MNW034, MNW102, and MNW107) analysed in this study can inhibit the urease enzyme. The progress curves results elucidate as the inhibition modality is based on a slow-binding mechanism. The initial rate experiment with the pre-incubation measures indicates a time-dependent inhibition based on a two-step isomerization mechanism; this evidence is supported by the SPU X-ray structure obtained from the urease inactivated by the MNW034 compounds (Luca Mazzei et al., 2019). Indeed, the structure reveals the presence of two Au atoms located in the proximity of the mobile helix-turn-helix motif (Luca Mazzei et al., 2019). This data, on the one hand, elucidate the basis of the compounds mediated inhibition as attributable to the disturbance of the mobile flap action that is fundamental for the urease activity. On the other hand, the lack of the organic ligand suggests a succession of different steps to obtain the compound-urease substitution and supports the kinetic results displaying the existence of an initial EI complex evolving in a more stable E*I complex. In the case of the bidentate N^N coordination compound, the EI complex may be explained by non-covalent gold-complex/urease interactions, responsible for the K_i at the initial inhibited state. Whereas the two Au ions bound to the Cys-His-Met urease's residues (Luca Mazzei et al., 2019) represent the E*I complex and produce the final inactivated state characterized by the K_i^*. Differently, the E*I complex obtained after urease inhibition with other Au(III)-based compounds is not yet characterized, and may contemplate retention of the cyclometallated ligands (Wenzel et al., 2018) (Luca Mazzei et al., 2019). Among those tested in this study, the cationic organic coordination compound (MNW034) exhibits the highest inhibitory activity. In contrast, the other neutral bidentate N^N compound (MNW102) shows a lower inhibitory efficiency as compared with the two C^N coordinating complexes (MNW033 and MNW107). The Au(III) C^N^N complex displays the least inhibition property, in agreement with its previously characterized low reactivity with other proteins (Meier, Gerner, Keppler, Cinellu, & Casini, 2016). The difference in efficacy between the two bidentate N^N compounds MNW034 and MNW102, cationic and neutral respectively, suggests a role as driving force in the initial phase for electrostatic interactions, which take place between the urease and the gold-complex, and are probably involved in the promotion of the Au(III) coordinative binding (Graziani et al., 2017) (Luca Mazzei et al., 2019).

Conclusions

This work highlights the potentiality of gold-based drugs to inhibit the urease enzyme, a virulence factor founded in a large variety of microorganisms, thanks to their ability to inactivate the enzyme in the low nanomolar concentration range. In 2017, ten out of the twelve antibiotic-resistant pathogens prioritized by the World Health Organization (WHO) for research of new antimicrobial strategies are ureolytic bacteria. Among these are *H. pylori, M. tuberculosis, C. neoformans*, and *Y. pestis*. Concluding, the promising results illustrated in this work can serve as an attractive starting point for future additional optimizations of the investigated gold compounds to obtain novel ureolytic-specific antibacterials.

Materials and methods

6.1.1 Enzyme and inhibitor sources

Canavalia ensifomis (jack bean) urease (JBU) (M_r = 250 kDa) C-3 powder (≥ 600,000 units/g) was purchased from Sigma-Aldrich SRL (St. Louis, MO). Enzyme quantification was carried out by measuring urease activity at pH 7.0 through a pH-STAT method (Stefano Benini, Gessa, & Ciurli, 1996), and considering the specific activities, JBU equal 3500 units (Krajewska, 2009). The inhibitors are synthetized by the laboratory of Prof. Angela Casini, Chair of Medicinal and Bioinorganic Chemistry, School of Chemistry, Cardiff University, Park Place, CF10 3AT Cardiff (United Kingdom).

6.1.2 Kinetics measurements

The experiments were performed at room temperature by using a spectrophotometric assay and an Agilent Cary 60 UV−vis spectrophotometer. The measurements were performed in a cresol red buffer solution (CR) containing 2 mM HEPES buffer, at pH 7.5, and 30 mg L^{-1} of cresol red, the latter being used as a pH indicator to monitor the increase in pH over time due to urease activity. All solutions were treated with CHELEX® resin (sodium form, 50-100 mesh, dry, Sigma Aldrich), following the manufacturer's instructions, in order to remove any trace of metal ions that could interfere with the enzymatic activity measurements. Stock solutions of compounds 1-5 (10 mM) were prepared by dissolving the powder in DMSO; 2 mM HEPES buffer, at pH 7.5 was used for further dilutions. Different concentrations of compounds 1-5, in the range 0-400 nM, were added to a 1 nM JBU solution dissolved in CR buffer.

6.1.2.1 Progress-curves assays

The experiments were started adding an enzyme and inhibitor solution to a concentrated solution of substrate urea to reach a final concentration of 100 mM. The change in absorbance at 573 nm, due to the pH-dependent change in the color of cresol red, was monitored over time every 10 s.

6.1.2.2 Initial rate experiments

The experiments were started adding an enzyme and inhibitor solution to a concentrated solution of substrate urea to reach a final concentration of 100 mM. The change in absorbance at 573 nm, due to the pH-dependent change in the color of cresol red, was monitored at different times. For each concentration of inhibitor, the initial reaction rate (v_i) was calculated as the slope of the linear portion of the absorbance versus time curves. The resulting values were normalized on the initial reaction rate in the absence of inhibitor (v_0), and the obtained percentage residual activity (RA, %) values were plotted as a function of the inhibitor concentration.

6.1.2.3 Pre-incubation experiments

After an appropriate incubation period (1-8 h), used for the enzyme–inhibitor complex to reach a steady-state condition, the experiments were started upon the addition of a concentrated solution of substrate urea to the incubation solution to reach a final concentration of 100 mM. The change in absorbance at 573 nm, due to the pH-dependent change in the color of cresol red, was monitored over time every 10 s. For each concentration of inhibitor, the initial reaction rate (v_i) was calculated as the slope of the linear portion of the absorbance versus time curves. The resulting values were normalized on the initial reaction rate in the absence of inhibitor (v_0), and the obtained percentage residual activity (RA, %) values were plotted as a function of the inhibitor concentration.

References

Aguinagalde, L., Díez-Martínez, R., Yuste, J., Royo, I., Gil, C., Lasa, Í., … Sánchez-Puelles, J. M. (2015). Auranofin efficacy against MDR Streptococcus pneumoniae and Staphylococcus aureus infections. *Journal of Antimicrobial Chemotherapy*. https://doi.org/10.1093/jac/dkv163

Andersen, M. T., Brøndsted, L., Pearson, B. M., Mulholland, F., Parker, M., Pin, C., … Ingmer, H. (2005). Diverse roles of HspR in Campylobacter jejuni revealed by the proteome, transcriptome and phenotypic characterization of an hspR mutant. *Microbiology*. https://doi.org/10.1099/mic.0.27513-0

Apel, D., Ellermeier, J., Pryjma, M., DiRita, V. J., & Gaynor, E. C. (2012). Characterization of Campylobacter jejuni RacRS reveals roles in the heat shock response, motility, and maintenance of cell length homogeneity. *Journal of Bacteriology*, *194*(9), 2342–2354. https://doi.org/10.1128/JB.06041-11

Avrain, L., Vernozy-Rozand, C., & Kempf, I. (2004). Evidence for natural horizontal transfer of tetO gene between Campylobacter jejuni strains in chickens. *Journal of Applied Microbiology*. https://doi.org/10.1111/j.1365-2672.2004.02306.x

Bailie, N. C., Osborne, C. A., Leininger, J. R., Fletcher, T. F., Johnston, S. D., Ogburn, P. N., & Griffith, D. P. (1986). Teratogenic effect of acetohydroxamic acid in clinically normal Beagles. *American Journal of Veterinary Research*.

Balasubramanian, A., & Ponnuraj, K. (2010). Crystal Structure of the First Plant Urease from Jack Bean: 83 Years of Journey from Its First Crystal to Molecular Structure. *Journal of Molecular Biology*. https://doi.org/10.1016/j.jmb.2010.05.009

Benini, S., Rypniewski, W. R., Wilson, K. S., Ciurli, S., & Mangani, S. (1998). The complex of Bacillus pasteurii urease with β-mercaptoethanol from X- ray data at 1.65-Å resolution. *Journal of Biological Inorganic Chemistry*. https://doi.org/10.1007/s007750050231

Benini, Stefano, Cianci, M., Mazzei, L., & Ciurli, S. (2014). Fluoride inhibition of Sporosarcina pasteurii urease: Structure and thermodynamics. *Journal of Biological Inorganic Chemistry*. https://doi.org/10.1007/s00775-014-1182-x

Benini, Stefano, Gessa, C., & Ciurli, S. (1996). Bacillus pasteurii urease: A heteropolymeric enzyme with a binuclear nickel active site. *Soil Biology and*

Biochemistry. https://doi.org/10.1016/0038-0717(96)00017-X

Benini, Stefano, Rypniewski, W. R., Wilson, K. S., Miletti, S., Ciurli, S., & Mangani, S. (1999). A new proposal for urease mechanism based on the crystal structures of the native and inhibited enzyme from Bacillus pasteurii: Why urea hydrolysis costs two nickels. *Structure*. https://doi.org/10.1016/S0969-2126(99)80026-4

Bindoli, A., Rigobello, M. P., Scutari, G., Gabbiani, C., Casini, A., & Messori, L. (2009). Thioredoxin reductase: A target for gold compounds acting as potential anticancer drugs. *Coordination Chemistry Reviews*. https://doi.org/10.1016/j.ccr.2009.02.026

Blaser, M. J. (1997). Epidemiologic and clinical features of Campylobacter jejuni infections. *The Journal of Infectious Diseases*.

Bucca, G., Brassington, A. M. E., Schönfeld, H. J., & Smith, C. P. (2000). The HspR regulon of Streptomyces coelicolor: A role for the DnaK chaperone as a transcriptional co-repressor. *Molecular Microbiology*. https://doi.org/10.1046/j.1365-2958.2000.02194.x

Bucca, G., Hindle, Z., & Smith, C. P. (1997). Regulation of the dnaK operon of Streptomyces coelicolor A3(2) is governed by HspR, an autoregulatory repressor protein. *Journal of Bacteriology*. https://doi.org/10.1128/jb.179.19.5999-6004.1997

Burne, R. A., & Chen, Y. Y. M. (2000). Bacterial ureases in infectious diseases. *Microbes and Infection*. https://doi.org/10.1016/S1286-4579(00)00312-9

Carrillo, C. D., Taboada, E., Nash, J. H. E., Lanthier, P., Kelly, J., Lau, P. C., … Szymanski, C. M. (2004). Genome-wide Expression Analyses of Campylobacter jejuni NCTC11168 Reveals Coordinate Regulation of Motility and Virulence by flhA. *Journal of Biological Chemistry*. https://doi.org/10.1074/jbc.M401134200

Clemens, D. L., Lee, B. Y., & Horwitz, M. A. (1995). Purification, characterization, and genetic analysis of Mycobacterium tuberculosis urease, a potentially critical determinant of host-pathogen interaction. *Journal of Bacteriology*. https://doi.org/10.1128/jb.177.19.5644-5652.1995

Coker, C., Poore, C. A., Li, X., & Mobley, H. L. T. (2000). Pathogenesis of proteus mirabilis urinary tract infection. *Microbes and Infection*. https://doi.org/10.1016/S1286-4579(00)01304-6

Collins, C. M., & D'Orazio, S. E. F. (1993). Bacterial ureases: structure, regulation of expression and role in pathogenesis. *Molecular Microbiology*.

https://doi.org/10.1111/j.1365-2958.1993.tb01220.x

Copeland, R. A. (2013). Evaluation of Enzyme Inhibitors in Drug Discovery. In *Evaluation of Enzyme Inhibitors in Drug Discovery*. https://doi.org/10.1002/9781118540398

Danielli, A., Amore, G., & Scarlato, V. (2010). Built shallow to maintain homeostasis and persistent infection: Insight into the transcriptional regulatory network of the gastric human pathogen Helicobacter pylori. *PLoS Pathogens*. https://doi.org/10.1371/journal.ppat.1000938

Das Gupta, T., Bandyopadhyay, B., & Das Gupta, S. K. (2008). Modulation of DNA-binding activity of Mycobacterium tuberculosis HspR by chaperones. *Microbiology*. https://doi.org/10.1099/mic.0.2007/012294-0

De Boer, P., Wagenaar, J. A., Achterberg, R. P., Van Putten, J. P. M., Schouls, L. M., & Duim, B. (2002). Generation of Campylobacter jejuni genetic diversity in vivo. *Molecular Microbiology*. https://doi.org/10.1046/j.1365-2958.2002.02930.x

Dugar, G., Herbig, A., Förstner, K. U., Heidrich, N., Reinhardt, R., Nieselt, K., & Sharma, C. M. (2013). High-Resolution Transcriptome Maps Reveal Strain-Specific Regulatory Features of Multiple Campylobacter jejuni Isolates. *PLoS Genetics*. https://doi.org/10.1371/journal.pgen.1003495

Eaton, K. A., Brooks, C. L., Morgan, D. R., & Krakowka, S. (1991). Essential role of urease in pathogenesis of gastritis induced by Helicobacter pylori in gnotobiotic piglets. *Infection and Immunity*.

Farrugia, M. A., Macomber, L., & Hausinger, R. P. (2013). Biosynthesis of the urease metallocenter. *Journal of Biological Chemistry*. https://doi.org/10.1074/jbc.R112.446526

Fernández, G. A., Vela Gurovic, M. S., Olivera, N. L., Chopa, A. B., & Silbestri, G. F. (2014). Antibacterial properties of water-soluble gold(I) N-heterocyclic carbene complexes. *Journal of Inorganic Biochemistry*. https://doi.org/10.1016/j.jinorgbio.2014.03.001

Grandvalet, C., De Crécy-Lagard, V., & Mazodier, P. (1999). The ClpB ATPase of Streptomyces albus G belongs to the HspR heat shock regulon. *Molecular Microbiology*. https://doi.org/10.1046/j.1365-2958.1999.01193.x

Graziani, V., Marrone, A., Re, N., Coletti, C., Platts, J. A., & Casini, A. (2017). A Multi-Level Theoretical Study to Disclose the Binding Mechanisms of Gold(III)–Bipyridyl Compounds as Selective Aquaglyceroporin Inhibitors. *Chemistry - A European Journal*. https://doi.org/10.1002/chem.201703092

Ha, N. C., Oh, S. T., Sung, J. Y., Cha, K. A., Lee, M. H., & Oh, B. H. (2001). Supramolecular assembly and acid resistance of Helicobacter pylori urease. *Nature Structural Biology*. https://doi.org/10.1038/88563

Hassane, D. C., Lee, R. B., & Pickett, C. L. (2003). Campylobacter jejuni cytolethal distending toxin promotes DNA repair responses in normal human cells. *Infection and Immunity*. https://doi.org/10.1128/IAI.71.1.541-545.2003

Hendrixson, D. R., & DiRita, V. J. (2004). Identification of Campylobacter jejuni genes involved in commensal colonization of the chick gastrointestinal tract. *Molecular Microbiology*. https://doi.org/10.1111/j.1365-2958.2004.03988.x

Holmes, C. W., Penn, C. W., & Lund, P. A. (2010). The hrcA and hspR regulons of Campylobacter jejuni. *Microbiology*. https://doi.org/10.1099/mic.0.031708-0

Hugdahl, M. B., Beery, J. T., & Doyle, M. P. (1988). Chemotactic behavior of Campylobacter jejuni. *Infection and Immunity*.

Jabri, E., Carr, M. B., Hausinger, R. P., & Karplus, P. A. (1995). The crystal structure of urease from Klebsiella aerogenes. *Science*. https://doi.org/10.1126/science.7754395

Jäger, S., Jäger, A., & Klug, G. (2004). CIRCE is not involved in heat-dependent transcription of groESL but in stabilization of the mRNA 5′-end in Rhodobacter capsulatus. *Nucleic Acids Research*. https://doi.org/10.1093/nar/gkh174

Kao, C. Y., Sheu, B. S., & Wu, J. J. (2016). Helicobacter pylori infection: An overview of bacterial virulence factors and pathogenesis. *Biomedical Journal*. https://doi.org/10.1016/j.bj.2015.06.002

Keerthisinghe, D. G., & Blakeley, R. L. (1995). Inhibition of jack bean urease by phosphoric-and thiophosphorictriamides. *Soil Biology and Biochemistry*. https://doi.org/10.1016/0038-0717(95)00002-V

Kosikowska, P., & Berlicki, Ł. (2011). Urease inhibitors as potential drugs for gastric and urinary tract infections: A patent review. *Expert Opinion on Therapeutic Patents*. https://doi.org/10.1517/13543776.2011.574615

Krajewska, B. (2008). Mono- (Ag, Hg) and di- (Cu, Hg) valent metal ions effects on the activity of jack bean urease. Probing the modes of metal binding to the enzyme. *Journal of Enzyme Inhibition and Medicinal Chemistry*. https://doi.org/10.1080/14756360701743051

Krajewska, B. (2009). Ureases I. Functional, catalytic and kinetic properties: A review.

Journal of Molecular Catalysis B: Enzymatic. https://doi.org/10.1016/j.molcatb.2009.01.003

Kumar, A., Grimes, B., Logan, M., Wedgwood, S., Williamson, H., & Hayward, R. S. (1995). A hybrid sigma subunit directs RNA polymerase to a hybrid promoter in Escherichia coli. *Journal of Molecular Biology*. https://doi.org/10.1016/S0022-2836(05)80105-6

Lara-Tejero, M., & Galan, J. E. (2000). A bacterial toxin that controls cell cycle progression as a deoxyribonuclease I-like protein. *Science*. https://doi.org/10.1126/science.290.5490.354

Linton, D., Gilbert, M., Hitchen, P. G., Dell, A., Morris, H. R., Wakarchuk, W. W., … Wren, B. W. (2000). Phase variation of a β-1,3 galactosyltransferase involved in generation of the ganglioside GM1-like lipo-oligosaccharide of Campylobacter jejuni. *Molecular Microbiology*. https://doi.org/10.1046/j.1365-2958.2000.02020.x

Liu, J., Huang, C., Shin, D. H., Yokota, H., Jancarik, J., Kim, J. S., … Kim, S. H. (2005). Crystal structure of a heat-inducible transcriptional repressor HrcA from Thermotoga maritima: Structural insight into DNA binding and dimerization. *Journal of Molecular Biology*. https://doi.org/10.1016/j.jmb.2005.04.021

Mazzei, L., Cianci, M., Musiani, F., & Ciurli, S. (2016). Inactivation of urease by 1,4-benzoquinone: Chemistry at the protein surface. *Dalton Transactions*. https://doi.org/10.1039/c6dt00652c

Mazzei, Luca, Cianci, M., Musiani, F., Lente, G., Palombo, M., & Ciurli, S. (2017). Inactivation of urease by catechol: Kinetics and structure. *Journal of Inorganic Biochemistry*. https://doi.org/10.1016/j.jinorgbio.2016.11.016

Mazzei, Luca, Wenzel, M. N., Cianci, M., Palombo, M., Casini, A., & Ciurli, S. (2019). Inhibition Mechanism of Urease by Au(III) Compounds Unveiled by X-ray Diffraction Analysis. *ACS Medicinal Chemistry Letters*, *10*(4), 564–570. https://doi.org/10.1021/acsmedchemlett.8b00585

McSweegan, E., & Walker, R. I. (1986). Identification and characterization of two Campylobacter jejuni adhesins for cellular and mucous substrates. *Infection and Immunity*.

Meier, S. M., Gerner, C., Keppler, B. K., Cinellu, M. A., & Casini, A. (2016). Mass Spectrometry Uncovers Molecular Reactivities of Coordination and Organometallic Gold(III) Drug Candidates in Competitive Experiments That Correlate with Their

Biological Effects. *Inorganic Chemistry*. https://doi.org/10.1021/acs.inorgchem.5b03000

Mignani, S. M., El Brahmi, N., El Kazzouli, S., Laurent, R., Ladeira, S., Caminade, A. M., … Majoral, J. P. (2017). Original Multivalent Gold(III) and Dual Gold(III)-Copper(II) Conjugated Phosphorus Dendrimers as Potent Antitumoral and Antimicrobial Agents. *Molecular Pharmaceutics*. https://doi.org/10.1021/acs.molpharmaceut.7b00771

Miller, E. F., & Maier, R. J. (2014). Ammonium metabolism enzymes aid Helicobacter pylori acid resistance. *Journal of Bacteriology*. https://doi.org/10.1128/JB.01423-13

Mobley, H. L. T., & Hausinger, R. P. (1989). Microbial ureases: Significance, regulation, and molecular characterization. *Microbiological Reviews*. https://doi.org/10.1128/mmbr.53.1.85-108.1989

Mobley, H. L. T., Island, M. D., & Hausinger, R. P. (1995). Molecular biology of microbial ureases. *Microbiological Reviews*.

Montecucco, C., & Rappuoli, R. (2001). Living dangerously: How helicobacter pylori survives in the human stomach. *Nature Reviews Molecular Cell Biology*. https://doi.org/10.1038/35073084

Morimoto, R. I. (1998). Regulation of the heat shock transcriptional response: Cross talk between a family of heat shock factors, molecular chaperones, and negative regulators. *Genes and Development*. https://doi.org/10.1101/gad.12.24.3788

Morita, M. T., Tanaka, Y., Kodama, T. S., Kyogoku, Y., Yanagi, H., & Yura, T. (1999). Translational induction of heat shock transcription factor σ 32 : Evidence for a built-in RNA thermosensor. *Genes and Development*. https://doi.org/10.1101/gad.13.6.655

Morrison, J. F., & Walsh, C. T. (1988). The behavior and significance of slow-binding enzyme inhibitors. *Advances in Enzymology and Related Areas of Molecular Biology*.

Morrison, John F. (1982). The slow-binding and slow, tight-binding inhibition of enzyme-catalysed reactions. *Trends in Biochemical Sciences*. https://doi.org/10.1016/0968-0004(82)90157-8

Munakata, K. ichi, Mochida, H., Kondo, S., & Suzuki, Y. (1980). Mutagenicity of N-acylglycinohydroxamic acids and related compounds. *Journal of Pharmacobio-Dynamics*. https://doi.org/10.1248/bpb1978.3.557

Nyati, K. K., & Nyati, R. (2013). Role of Campylobacter jejuni Infection in the Pathogenesis of Guillain-Barré Syndrome: An Update . *BioMed Research International*. https://doi.org/10.1155/2013/852195

Owings, J. P., McNair, N. N., Mui, Y. F., Gustafsson, T. N., Holmgren, A., Contel, M., … Mead, J. R. (2016). Auranofin and N-heterocyclic carbene gold-analogs are potent inhibitors of the bacteria Helicobacter pylori. *FEMS Microbiology Letters*. https://doi.org/10.1093/femsle/fnw148

Parijat, P., & Batra, J. K. (2015). Role of DnaK in HspR-HAIR interaction of Mycobacterium tuberculosis. *IUBMB Life*. https://doi.org/10.1002/iub.1438

Parkhill, J., Wren, B. W., Mungall, K., Ketley, J. M., Churcher, C., Basham, D., … Barrell, B. G. (2000). The genome sequence of the food-borne pathogen Campylobacter jejuni reveals hypervariable sequences. *Nature*. https://doi.org/10.1038/35001088

Pepe, S., Pinatel, E., Fiore, E., Puccio, S., Peano, C., Brignoli, T., … Roncarati, D. (2018). The Helicobacter pylori heat-shock repressor HspR: Definition of its direct regulon and characterization of the cooperative DNA-binding mechanism on its own promoter. *Frontiers in Microbiology*. https://doi.org/10.3389/fmicb.2018.01887

Perez, J. C., & Groisman, E. A. (2009). Evolution of Transcriptional Regulatory Circuits in Bacteria. *Cell*. https://doi.org/10.1016/j.cell.2009.07.002

Pope, A. J., Toseland, C. D. N., Rushant, B., Richardson, S., Mcvey, M., & Hills, J. (1998). Effect of potent urease inhibitor, fluorofamide, on Helicobacter sp. in vivo and in vitro. *Digestive Diseases and Sciences*. https://doi.org/10.1023/A:1018884322973

Roder, C., & Thomson, M. J. (2015). Auranofin: Repurposing an Old Drug for a Golden New Age. *Drugs in R and D*. https://doi.org/10.1007/s40268-015-0083-y

Roncarati, D., Danielli, A., & Scarlato, V. (2011). Cbpa acts as a modulator of HspR repressor DNA binding activity in Helicobacter pylori. *Journal of Bacteriology*. https://doi.org/10.1128/JB.05295-11

Roncarati, D., Danielli, A., & Scarlato, V. (2014). The HrcA repressor is the thermosensor of the heat-shock regulatory circuit in the human pathogen Helicobacter pylori. *Molecular Microbiology*. https://doi.org/10.1111/mmi.12600

Roncarati, D., Danielli, A., Spohn, G., Delany, I., & Scarlato, V. (2007). Transcriptional regulation of stress response and motility functions in Helicobacter pylori is mediated by HspR and HrcA. *Journal of Bacteriology*. https://doi.org/10.1128/JB.00626-07

Roncarati, D., & Scarlato, V. (2017). Regulation of heat-shock genes in bacteria: from signal sensing to gene expression output. *FEMS Microbiology Reviews*. https://doi.org/10.1093/femsre/fux015

Roncarati, D., Spohn, G., Tango, N., Danielli, A., Delany, I., & Scarlato, V. (2007). Expression, purification and characterization of the membrane-associated HrcA repressor protein of Helicobacter pylori. *Protein Expression and Purification*. https://doi.org/10.1016/j.pep.2006.08.002

Sannella, A. R., Casini, A., Gabbiani, C., Messori, L., Bilia, A. R., Vincieri, F. F., … Severini, C. (2008). New uses for old drugs. Auranofin, a clinically established antiarthritic metallodrug, exhibits potent antimalarial effects in vitro: Mechanistic and pharmacological implications. *FEBS Letters*. https://doi.org/10.1016/j.febslet.2008.02.028

Schmidt, A., Schiesswohl, M., Volker, U., Hecker, M., & Schumann, W. (1992). Cloning, sequencing, mapping, and transcriptional analysis of the groESL operon from Bacillus subtilis. *Journal of Bacteriology*. https://doi.org/10.1128/jb.174.12.3993-3999.1992

Schmidt, C., Karge, B., Misgeld, R., Prokop, A., Brönstrup, M., & Ott, I. (2017). Biscarbene gold(i) complexes: Structure-activity-relationships regarding antibacterial effects, cytotoxicity, TrxR inhibition and cellular bioavailability. *MedChemComm*. https://doi.org/10.1039/c7md00269f

Schoep, T. D., Fulurija, A., Good, F., Lu, W., Himbeck, R. P., Schwan, C., … Marshall, B. J. (2010). Surface properties of Helicobacter pylori urease complex are essential for persistence. *PLoS ONE*. https://doi.org/10.1371/journal.pone.0015042

Schumann, W., Homuth, G., & Mogk, A. (1998). The GroE chaperonin machine is the major modulator of the CIRCE heat shock regulon of Bacillus subtilis. *Journal of Biosciences*. https://doi.org/10.1007/BF02936135

Schwartz, J. T. (2006). Role of urease in megasome formation and Helicobacter pylori survival in macrophages. *Journal of Leukocyte Biology*. https://doi.org/10.1189/jlb.0106030

Scott, D. R., Marcus, E. A., Wen, Y., Singh, S., Feng, J., & Sachs, G. (2010). Cytoplasmic histidine kinase (HP0244)-regulated assembly of urease with UreI, a channel for urea and its metabolites, CO2, NH3, and NH4+, is necessary for acid survival of Helicobacter pylori. *Journal of Bacteriology*. https://doi.org/10.1128/JB.00848-09

Seshasayee, A. S., Bertone, P., Fraser, G. M., & Luscombe, N. M. (2006). Transcriptional regulatory networks in bacteria: from input signals to output responses. *Current Opinion in Microbiology*. https://doi.org/10.1016/j.mib.2006.08.007

Sharp, M. M., Chan, C. L., Lu, C. Z., Marr, M. T., Nechaev, S., Merritt, E. W., … Gross, C. A. (1999). The interface of σ with core RNA polymerase is extensive, conserved, and functionally specialized. *Genes and Development*. https://doi.org/10.1101/gad.13.22.3015

Spohn, G., Danielli, A., Roncarati, D., Delany, I., Rappuoli, R., & Scarlato, V. (2004). Dual Control of Helicobacter pylori Heat Shock Gene Transcription by HspR and HrcA. *Journal of Bacteriology*. https://doi.org/10.1128/JB.186.10.2956-2965.2004

Stewart, G. R., Wernisch, L., Stabler, R., Mangan, J. A., Hinds, J., Laing, K. G., … Butcher, P. D. (2002). Dissection of the heat-shock response in Mycobacterium tuberculosis using mutants and microarrays. *Microbiology*.

Tanaka, T., Kawase, M., & Tani, S. (2004). α-Hydroxyketones as inhibitors of urease. *Bioorganic and Medicinal Chemistry*. https://doi.org/10.1016/j.bmc.2003.10.017

Thies, F. L., Karch, H., Hartung, H. P., & Giegerich, G. (1999). Cloning and expression of the dnaK gene of Campylobacter jejuni and antigenicity of heat shock protein 70. *Infection and Immunity*.

Tomoyasu, T., Ogura, T., Tatsuta, T., & Bukau, B. (1998). Levels of DnaK and DnaJ provide tight control of heat shock gene expression and protein repair in Escherichia coli. *Molecular Microbiology*. https://doi.org/10.1046/j.1365-2958.1998.01090.x

Vassiliou, S., Grabowiecka, A., Kosikowska, P., Yiotakis, A., Kafarski, P., & Berlicki, L. (2008). Design, synthesis, and evaluation of novel organophosphorus inhibitors of bacterial ureases. *Journal of Medicinal Chemistry*. https://doi.org/10.1021/jm800570q

Warzajtis, B., Glišić, B. D., Savić, N. D., Pavic, A., Vojnovic, S., Veselinović, A., … Djuran, M. I. (2017). Mononuclear gold(iii) complexes with l-histidine-containing dipeptides: tuning the structural and biological properties by variation of the N-terminal amino acid and counter anion. *Dalton Transactions*. https://doi.org/10.1039/c6dt04862e

Weeks, D. L., Eskandari, S., Scott, D. R., & Sachs, G. (2000). A H+-gated urea channel: The link between Helicobacter pylori urease and gastric colonization. *Science*. https://doi.org/10.1126/science.287.5452.482

Wenzel, M. N., Meier-Menches, S. M., Williams, T. L., Rämisch, E., Barone, G., & Casini, A.

(2018). Selective targeting of PARP-1 zinc finger recognition domains with Au(III) organometallics. *Chemical Communications*. https://doi.org/10.1039/c7cc08406d

Wilson, A. C., & Tan, M. (2004). Stress response gene regulation in Chlamydia is dependent on HrcA-CIRCE Interactions. *Journal of Bacteriology*. https://doi.org/10.1128/JB.186.11.3384-3391.2004

Yao, R., Burr, D. H., & Guerry, P. (1997). CheY-mediated modulation of campylobacter jejuni virulence. *Molecular Microbiology*. https://doi.org/10.1046/j.1365-2958.1997.2861650.x

Young, K. T., Davis, L. M., & DiRita, V. J. (2007). Campylobacter jejuni: Molecular biology and pathogenesis. *Nature Reviews Microbiology*, *5*(9), 665–679. https://doi.org/10.1038/nrmicro1718

Zambelli, B., Musiani, F., Benini, S., & Ciurli, S. (2011). Chemistry of Ni2+ in urease: Sensing, trafficking, and catalysis. *Accounts of Chemical Research*. https://doi.org/10.1021/ar200041k